

Field dependent quasiparticles in models of strongly correlated electrons

J. Bauer and A.C. Hewson

Department of Mathematics, Imperial College, London SW7 2AZ, United Kingdom

(Dated: July 15, 2018)

In earlier work we showed how the low energy behavior of the symmetric Anderson model in a magnetic field H could be described in terms of field dependent renormalized quasiparticles. Here we extend the approach to the non-symmetric Anderson impurity model and to the infinite dimensional Hubbard model within the DMFT approach. We present NRG results for the local spectral densities and the local longitudinal and transverse dynamic spin susceptibilities for different parameter regimes and a sequence of values of the magnetic field. We calculate renormalized parameters which characterize the quasiparticle excitations. Away from half-filling we find quasiparticle weights, $z_\sigma(H)$, which differ according to the spin type $\sigma = \uparrow$ or $\sigma = \downarrow$. Using the renormalized perturbation theory, we show that the low energy features in the NRG results can be well described in the metallic phase in terms of these field dependent parameters. We also check Luttinger's theorem for the Hubbard model and find it to be satisfied in all parameter regimes and for all values of the magnetic field.

PACS numbers: 72.15.Qm, 75.20.Hr, 73.21.La

I. INTRODUCTION

A feature of strongly correlated electron systems, such as heavy fermions, is their sensitivity to an applied magnetic field, which makes a magnetic field a useful experimental probe of strong correlation behavior. A manifestation of this sensitivity is the very large paramagnetic susceptibility observed in these systems. In terms of Fermi liquid theory, the large paramagnetic susceptibility can be interpreted as due to quasiparticles with exceptionally large effective masses. These large effective masses arise from the scattering of the electrons with the enhanced spin fluctuations induced by the strong local Coulomb interactions. An applied magnetic field suppresses the spin fluctuations causing a reduction in the effective masses, which can be seen experimentally in de Haas-van Alphen measurements^{1,2}. Not only do the effective masses depend on the magnetic field, they may also differ for the spin up and spin down electrons^{3,4}. Another feature that reflects the enhanced sensitivity to an applied field is metamagnetic behavior, where the spin susceptibility $\chi(H)$ in a finite field H increases with the field strength such that $d\chi(H)/dH > 0$, which has been observed in some heavy fermion compounds⁵. As a related feature it has also been predicted that strong magnetic fields can induce localization in narrow conduction bands^{6,7,8}, and this has been observed experimentally in quasi-two dimensional organic conductors⁹.

In an earlier paper¹⁰, we looked at local models of strong correlation behavior in a magnetic field and showed how the quasiparticles can be described by field-dependent renormalized parameters. We based our approach on the single impurity Anderson model¹¹, which can be characterized by the three independent parameters, ε_d , the impurity level, Δ , the broadening of this level due to the hybridization with conduction electrons, and U , the interaction at the impurity site. In the absence of a magnetic field, the low energy quasiparticle

excitations can be described by an effective version of the same model with three corresponding renormalized parameters, $\tilde{\varepsilon}_d$, $\tilde{\Delta}$, and \tilde{U} ^{12,13,14}. We have shown that, in the presence of a magnetic field H , these parameters can be taken as field-dependent, $\tilde{\varepsilon}_{d,\sigma}(H)$, $\tilde{\Delta}_\sigma(H)$, and $\tilde{U}(H)$. For the particle-hole symmetric model, we calculated the H -dependence explicitly from numerical renormalization group (NRG) calculations of the low energy excitations^{10,14}. The process of de-renormalization of the quasiparticles with increase of magnetic field can be followed in these results. The parameters which describe the quasiparticles change slowly on increasing the field from zero and revert to their uncorrelated mean field values in the extreme high field limit.

The renormalized parameters are not just a convenient way of describing the low energy behavior; they completely specify the model. A renormalized perturbation theory (RPT) can be set up in which the free propagators correspond to fully dressed quasiparticles^{15,16}. This formalism is particularly effective for describing the Fermi liquid regime, as only diagrams up to second order have to be taken into account to obtain asymptotically exact results for the $T = 0$ susceptibilities, and the leading T^2 term in the conductivity. This perturbation expansion is not restricted to the low energy and low temperature regime, and can be used for calculations on all energy scales. We have shown that a very good description of the $T = 0$ spin and charge dynamics for the Anderson model in the Kondo regime can be obtained by summing the RPT diagrams for repeated quasiparticle scattering¹⁷. The results give an accurate description of the spin and charge susceptibilities for arbitrary magnetic field values H , and for frequencies ω extending over a range significantly larger than the Kondo temperature T_K . The Korringa-Shiba relation¹⁸ and the sum rules for the spectral density are satisfied.

In this paper we further extend this renormalized parameter approach to infinite dimensional lattice models,

concentrating particularly on the Hubbard model. However, before doing so, we generalize some of our earlier results for the Anderson model to situations away particle-hole symmetry. We do this not only for the sake of completeness but also so we can make a comparison with the results for the lattice model in this regime.

II. THE NON-SYMMETRIC ANDERSON MODEL IN A MAGNETIC FIELD

The Hamiltonian for the Anderson model¹¹ is

$$H_{\text{AM}} = \sum_{\sigma} \varepsilon_{\text{d},\sigma} d_{\sigma}^{\dagger} d_{\sigma} + U n_{\text{d},\uparrow} n_{\text{d},\downarrow} + \sum_{k,\sigma} (V_{k,\sigma} d_{\sigma}^{\dagger} c_{k,\sigma} + V_{k,\sigma}^{*} c_{k,\sigma}^{\dagger} d_{\sigma}) + \sum_{k,\sigma} \varepsilon_{k,\sigma} c_{k,\sigma}^{\dagger} c_{k,\sigma}, \quad (1)$$

where $\varepsilon_{\text{d},\sigma} = \varepsilon_{\text{d}} - \sigma g \mu_{\text{B}} H/2$ is the energy of the localized level at an impurity site in a magnetic field H , U the interaction at this local site, and $V_{k,\sigma}$ the hybridization matrix element to a band of conduction electrons of spin σ with energy $\varepsilon_{k,\sigma} - \sigma g_c \mu_{\text{B}} H/2$, where g_c is the g -factor for the conduction electrons. When $U = 0$ the local level broadens into a resonance, corresponding to a localized quasi-bound state, whose width depends on the quantity $\Delta_{\sigma}(\omega) = \pi \sum_k |V_{k,\sigma}|^2 \delta(\omega - \varepsilon_{k,\sigma})$. For the impurity model, where we are interested in universal features, it is usual to take a wide conduction band with a flat density of states so that $\Delta_{\sigma}(\omega)$ becomes independent of ω , and can be taken as a constant Δ_{σ} . In this wide band limit $\Delta_{\sigma}(\omega)$ will be independent of the magnetic field on the conduction electrons, so we can effectively put $g_c = 0$. When this is the case Δ_{σ} is usually taken to be a constant Δ independent of σ .

In the renormalized perturbation theory approach^{15,16} we cast the corresponding Lagrangian for this model $\mathcal{L}_{\text{AM}}(\varepsilon_{\text{d},\sigma}, \Delta, U)$ into the form,

$$\mathcal{L}_{\text{AM}}(\varepsilon_{\text{d},\sigma}, \Delta, U) = \mathcal{L}_{\text{AM}}(\tilde{\varepsilon}_{\text{d},\sigma}, \tilde{\Delta}_{\sigma}, \tilde{U}) + \mathcal{L}_{\text{ct}}(\lambda_1, \lambda_2, \lambda_3), \quad (2)$$

where the renormalized parameters, $\tilde{\varepsilon}_{\text{d},\sigma}$ and $\tilde{\Delta}_{\sigma}$, are defined in terms of the self-energy $\Sigma_{\sigma}(\omega)$ of the one-electron Green function for the impurity state,

$$G_{\sigma}(\omega) = \frac{1}{\omega - \varepsilon_{\text{d},\sigma} + i\Delta - \Sigma_{\sigma}(\omega)}, \quad (3)$$

and are given by

$$\tilde{\varepsilon}_{\text{d},\sigma} = z_{\sigma}(\varepsilon_{\text{d},\sigma} + \Sigma_{\sigma}(0)), \quad \tilde{\Delta}_{\sigma} = z_{\sigma}\Delta, \quad (4)$$

where z_{σ} is given by $z_{\sigma} = 1/(1 - \Sigma'_{\sigma}(0))$. The renormalized or quasiparticle interaction \tilde{U} , is defined in terms of the local total 4-vertex $\Gamma_{\uparrow\downarrow}(\omega_1, \omega_2, \omega_3, \omega_4)$ at zero frequency,

$$\tilde{U} = z_{\uparrow} z_{\downarrow} \Gamma_{\uparrow\downarrow}(0, 0, 0, 0). \quad (5)$$

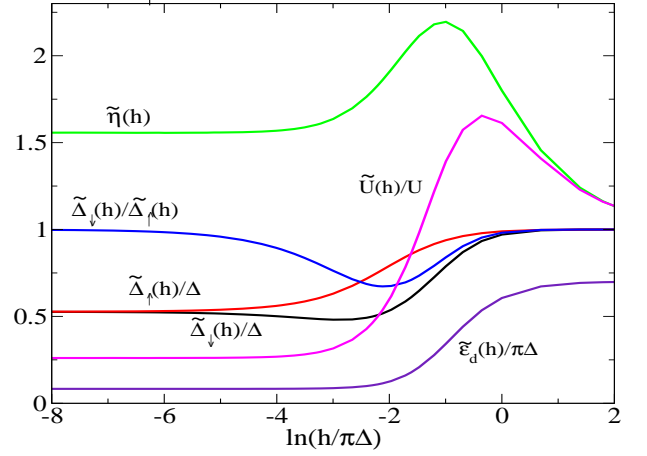


FIG. 1: Plots of the renormalized parameters, $\tilde{\Delta}_{\uparrow}(h)/\Delta$, $\tilde{\Delta}_{\downarrow}(h)/\Delta$, $\tilde{\varepsilon}_{\text{d}}(h)/\pi\Delta$, $\tilde{U}(h)/U$, $\tilde{\eta}(h)$, for the asymmetric Anderson model, with $\pi\Delta = 0.1$, $U/\pi\Delta = 2$ and $\varepsilon_{\text{d}}/\pi\Delta = -0.3$, as a function of the logarithm of the magnetic field $h/\pi\Delta$. The ratio $\tilde{\Delta}_{\downarrow}(h)/\tilde{\Delta}_{\uparrow}(h)$ is also shown.

It will be convenient to rewrite the spin dependent quasiparticle energies in the form, $\tilde{\varepsilon}_{\text{d},\sigma} = \tilde{\varepsilon}_{\text{d}}(h) - \sigma h \tilde{\eta}(h)$, where

$$\tilde{\varepsilon}_{\text{d}}(h) = \frac{1}{2} \sum_{\sigma} \tilde{\varepsilon}_{\text{d},\sigma}, \quad \tilde{\eta}(h) = \frac{1}{2h} \sum_{\sigma} \sigma \tilde{\varepsilon}_{\text{d},\sigma} \quad (6)$$

where $\tilde{\varepsilon}_{\text{d}}(h)$ and $\tilde{\eta}(h)$ are both even functions of the magnetic field $h = g \mu_{\text{B}} H/2$.

The renormalized perturbation expansion is in powers of the renormalized interaction \tilde{U} for the complete Lagrangian defined in equation (2). The counter term part of the Lagrangian $\mathcal{L}_{\text{ct}}(\lambda_1, \lambda_2, \lambda_3)$ essentially takes care of any overcounting. The parameters, $\tilde{\varepsilon}_{\text{d},\sigma}$, $\tilde{\Delta}_{\sigma}$ and \tilde{U} , have been taken to be the fully renormalized ones, and the counter term parameters, λ_1 , λ_2 and λ_3 , are required to cancel any further renormalization. They are completely determined by this condition.

We can calculate the renormalized parameters by identifying the Lagrangian $\mathcal{L}_{\text{AM}}(\tilde{\varepsilon}_{\text{d},\sigma}, \tilde{\Delta}_{\sigma}, \tilde{U})$ on the right hand side of equation (2) with the leading corrections to the fixed point in a numerical renormalization group calculation for the same model^{14,15,19,20}. Results for the general model in the absence of a magnetic field¹², and for the symmetric model in the presence of a field, were given earlier¹⁰. There are some significant differences for the case of a magnetic field in situations without particle-hole symmetry which will describe here briefly. The main difference is that the wavefunction renormalization factor $z_{\sigma}(h)$ depends on the spin index σ , and as a consequence so does the effective resonance width $\tilde{\Delta}_{\sigma}(h)$, so the equations given earlier for the particle-hole symmetric model¹⁰ have to be generalized. The induced magnetization $M(h)$ is given by $M(h) = g \mu_{\text{B}} m(h)$, where

$$m(h) = \frac{1}{2} (n_{\text{d}\uparrow} - n_{\text{d}\downarrow}) = \frac{-1}{2\pi} \sum_{\sigma} \sigma \tan^{-1} \left(\frac{\tilde{\varepsilon}_{\text{d},\sigma}(h)}{\tilde{\Delta}_{\sigma}(h)} \right), \quad (7)$$

which can be derived from the Friedel sum rule. The longitudinal susceptibility $\chi_l(h)$ (in units of $(g\mu_B)^2$) is given by

$$\chi_l(h) = 0.25(\tilde{\rho}_\uparrow(0, h) + \tilde{\rho}_\downarrow(0, h) + \tilde{U}(h)\tilde{\rho}_\uparrow(0, h)\tilde{\rho}_\downarrow(0, h)), \quad (8)$$

where $\tilde{\rho}_\sigma(\omega, h)$ is the free quasiparticle density of states given by

$$\tilde{\rho}_\sigma(\omega, h) = \frac{1}{\pi} \frac{\tilde{\Delta}_\sigma(h)}{(\omega - \tilde{\varepsilon}_{d,\sigma}(h))^2 + \tilde{\Delta}_\sigma^2(h)}. \quad (9)$$

The corresponding transverse susceptibility $\chi_t(h)$ (zero applied field limit in the transverse direction) is given by

$$\chi_t(h) = \frac{m(h)}{2h}. \quad (10)$$

The total occupation of the impurity site $n(h) = (n_{d\uparrow} + n_{d\downarrow})$ can be derived similarly, and is given by

$$n(h) = 1 - \frac{1}{2\pi} \sum_\sigma \tan^{-1} \left(\frac{\tilde{\varepsilon}_{d\sigma}(h)}{\tilde{\Delta}_\sigma(h)} \right), \quad (11)$$

and the local charge susceptibility $\chi_c(h)$ is given by

$$\chi_c(h) = 0.25[\tilde{\rho}_\uparrow(0, h) + \tilde{\rho}_\downarrow(0, h) - \tilde{U}(h)\tilde{\rho}_\uparrow(0, h)\tilde{\rho}_\downarrow(0, h)]. \quad (12)$$

In figure 1 we display the renormalized parameters as a function of the magnetic field on a log scale for the bare parameters $\varepsilon_d/\pi\Delta = -0.3$ and $U/\pi\Delta = 2$, corresponding to a impurity occupation in the absence of a field, $\langle n_{d,\sigma} \rangle = n(0)/2 \sim 0.35$. The overall trend is very similar to that for the particle-hole symmetric case in the strong coupling regime. We do see, however, that $\Delta_\uparrow(h) \neq \Delta_\downarrow(h)$, except asymptotically as $h \rightarrow 0$ and $h \rightarrow \infty$. We note that, though $\tilde{\Delta}_\uparrow(h)$ increases monotonically with increase of h , $\tilde{\Delta}_\downarrow(h)$ initially decreases. In this case, where the impurity level is less than half-filled, the ratio $\tilde{\Delta}_\uparrow(h)/\tilde{\Delta}_\downarrow(h) \geq 1$. This ratio is reversed, so $\tilde{\Delta}_\uparrow(h)/\tilde{\Delta}_\downarrow(h) \leq 1$, when the impurity level is more than half-filled. Shown in figure 2 is the result for $m(h)$ derived by substituting these parameters into equation (7), compared with results obtained by the direct evaluation of the d-site occupation values in the ground state as determined from the NRG. There is a small but systematic difference, of the order of 2%, between the two sets of results. The corresponding estimates of the average occupation number $n(h)/2$ as a function of magnetic field h are shown in the same figure. For this quantity the two sets of results are almost indistinguishable. In the extreme large field limit the average occupation of the impurity level tends to unity, as the majority spin level gets pulled further and further below the Fermi level, and the impurity becomes completely polarized. In this regime the average renormalized level, $\tilde{\varepsilon}_d$, approaches the mean field value, $\tilde{\varepsilon}_d = \varepsilon_d + 0.5Un(h)$, rather than the bare value ε_d , while the other renormalized quantities approach their bare values.

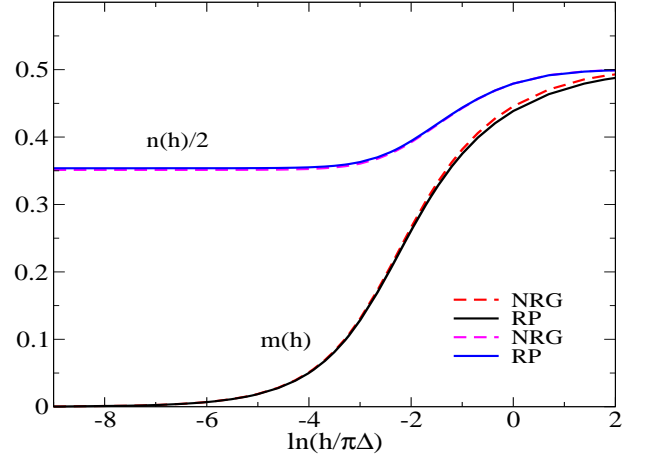


FIG. 2: The induced magnetization $m(h)$ as a function of the logarithm of the magnetic field h for the asymmetric Anderson model with the same set of parameters as given in figure 1. The dashed curve is that calculated from the direct evaluation of the occupation values from the NRG ground state, and the full curve is that deduced from the renormalized parameters in equation (7). Also shown is the average occupation $n(h)/2$ as calculated from the NRG ground state (dashed curve) and the quasiparticle occupation values (full curve) as given in equation (11).

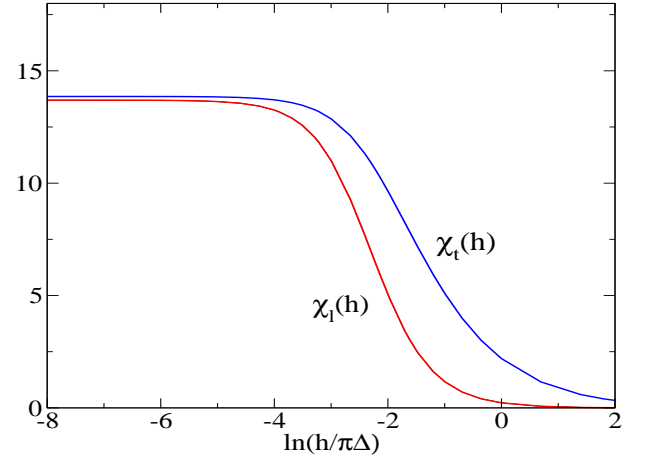


FIG. 3: The longitudinal and transverse impurity site susceptibilities, $\chi_l(h)$ and $\chi_t(h)$, as a function of the logarithm of the magnetic field h for the asymmetric Anderson model with the same set of parameters as given in figure 1. $\chi_l(h)$ is calculated from equation (8) and $\chi_t(h) = m(h)/2h$.

The longitudinal and transverse spin susceptibilities, $\chi_l(h)$ and $\chi_t(h)$, are plotted in figure 3 as a function of the logarithm of the magnetic field h . $\chi_l(h)$ is calculated from equation (8) and $\chi_t(h) = m(h)/2h$ as calculated from equation (7). They should asymptotically converge to the same result in the limit $h \rightarrow 0$. There seems to be a very small discrepancy, of about 1%, between the two estimates in this limit.

The generalization of our earlier results¹⁷ for the dy-

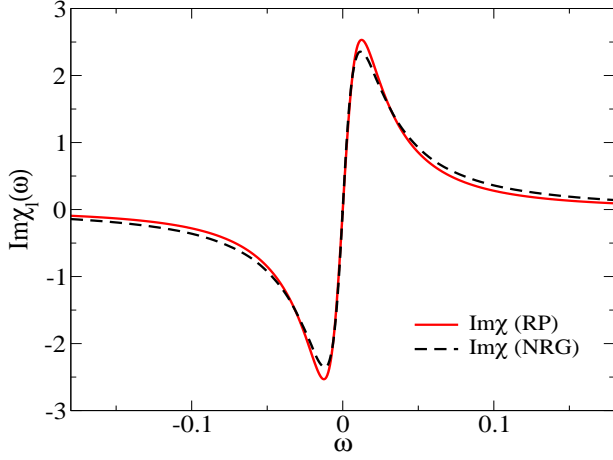


FIG. 4: The imaginary part of the longitudinal dynamic susceptibility, $\chi_l(\omega, h)$ at $T = 0$ as a function of ω , for the asymmetric Anderson model for $h/\pi\Delta = 0.001$, and the same set of parameters as given in figure 1. The dashed curve is calculated from a direct NRG calculation and the full curve from equation (13) with the renormalized parameters.

dynamic longitudinal susceptibility $\chi_l(\omega, h)$, taking account of repeated quasiparticle-quasihole scattering, is

$$\chi_l(\omega, h) = \frac{\tilde{\chi}_{\uparrow\uparrow}(\omega, h) + \tilde{\chi}_{\downarrow\downarrow}(\omega, h) + 4\tilde{U}_l(h)\tilde{\chi}_{\uparrow\uparrow}(\omega, h)\tilde{\chi}_{\downarrow\downarrow}(\omega, h)}{2(1 - 4\tilde{U}_l^2(h)\tilde{\chi}_{\uparrow\uparrow}(\omega, h)\tilde{\chi}_{\downarrow\downarrow}(\omega, h))}, \quad (13)$$

where the analytic expression for $\tilde{\chi}_{\sigma\sigma}(\omega, h)$ is given in the Appendix. The zero frequency irreducible particle-hole vertex $\tilde{U}_l(h)$ in this scattering channel is given by

$$\tilde{U}_l(h) = \frac{-1 + \sqrt{[1 + \tilde{U}^2(h)(\tilde{\rho}_{\uparrow} + \tilde{\rho}_{\downarrow})]^2 - \tilde{U}^2(h)(\tilde{\rho}_{\uparrow} - \tilde{\rho}_{\downarrow})^2}}{2(\tilde{\rho}_{\uparrow} + \tilde{\rho}_{\downarrow} + \tilde{U}(h)\tilde{\rho}_{\uparrow}\tilde{\rho}_{\downarrow})}, \quad (14)$$

where we have simplified the notation, $\tilde{\rho}_{\sigma}(0, h) = \tilde{\rho}_{\sigma}$. In the absence of a magnetic field, or with a magnetic field for the particle-hole symmetric model, $\tilde{\rho}_{\uparrow} = \tilde{\rho}_{\downarrow}$, the result simplifies to $\tilde{U}_l(h) = \tilde{U}(h)/[1 + \tilde{U}(h)\tilde{\rho}(0, h)]$, which is the value used in the earlier work¹⁷.

The imaginary part of the longitudinal dynamic susceptibility is shown in figure 4 for a magnetic field value $h/\pi\Delta = 0.001$ for the same set of parameters, as for figures 2 and 3. The dashed curve is that from a direct NRG evaluation^{21,22} and the full curve is that calculated using equation (13), with the corresponding renormalized parameters. In the direct NRG evaluation we have used the improved method^{23,24} of evaluating the response functions with the complete Anders-Schiller basis²⁵ so that the sum rule for the total spectral density is satisfied exactly. There is very good agreement between the two sets of results. The Korrington-Shiba relation does not hold for the model without particle-hole symmetry in the presence of a magnetic field. Where it does hold, in the absence of a field, or with particle-hole symmetry, the

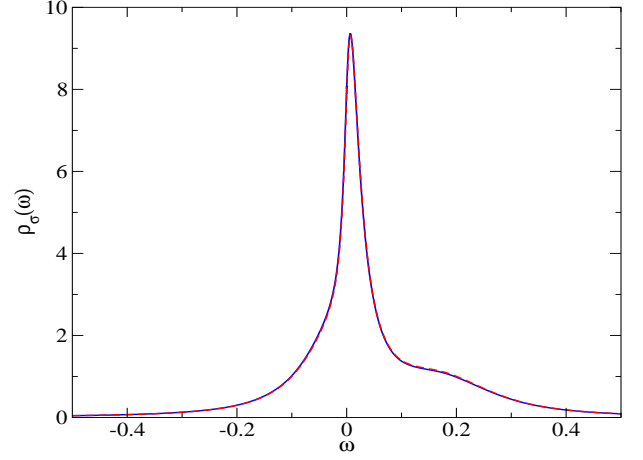


FIG. 5: The spectral density for the spin up (majority) electrons $\rho_{\uparrow}(\omega, h)$ (full curve) and spin down (minority) electrons $\rho_{\downarrow}(\omega, h)$ (dashed curve) at $T = 0$ as a function of ω for the same set parameters and magnetic field value as used for the plot of $\chi_l(\omega, h)$ in figure 4. The two curves are almost coincident on the scale shown.

renormalized perturbation expression satisfies it exactly. The spectral densities, $\rho_{\uparrow}(\omega)$ and $\rho_{\downarrow}(\omega)$, as calculated from the NRG for this field value and the same set of parameters, are shown in figure 5. For this value of the field there are only a small differences between the two spectral densities; they are almost coincident on the scale shown.

The dynamic transverse susceptibility $\chi_t(\omega, h)$, taking into account the quasiparticle-quasihole repeated scattering, is given by

$$\chi_t(\omega, h) = \frac{\tilde{\chi}_{\uparrow\downarrow}(\omega, h)}{1 - \tilde{U}_t(h)\tilde{\chi}_{\uparrow\downarrow}(\omega, h)}, \quad (15)$$

where the analytic expression for $\tilde{\chi}_{\uparrow\downarrow}(\omega, h)$ is given in the Appendix. The zero frequency irreducible particle-hole vertex $\tilde{U}_t(h)$ in this channel is

$$\tilde{U}_t(h) = \frac{1}{m(h)} \left\{ \frac{4\tilde{h}^2 + (\tilde{\Delta}_{\uparrow} - \tilde{\Delta}_{\downarrow})^2}{4\tilde{h} + \frac{(\tilde{\Delta}_{\uparrow} - \tilde{\Delta}_{\downarrow})}{2\pi m(h)} \ln \left(\frac{(\tilde{h} - \tilde{\epsilon}_d)^2 + \tilde{\Delta}_{\uparrow}^2}{(\tilde{h} + \tilde{\epsilon}_d)^2 + \tilde{\Delta}_{\downarrow}^2} \right)} - h \right\}, \quad (16)$$

where $\tilde{h} = h\tilde{\eta}(h)$, and $m(h)$ is given in equation (7). This expression simplifies in the case, $\tilde{\Delta}_{\uparrow} = \tilde{\Delta}_{\downarrow}$, to give $\tilde{U}_t(h) = (\tilde{h} - h)/m(h)$, which is the same as that used earlier¹⁷.

Apart from a factor of 2, the dynamic transverse susceptibility in weak fields is similar in form to the longitudinal one. In stronger fields, however, one of the peaks in the imaginary part is suppressed while the other peak is enhanced. Results are shown for the imaginary part of $\chi_t(\omega, h)$ in figure 6 for a field value $h/\pi\Delta = 0.04$ and the same parameters as for figures 2-5.

The full curve gives the results derived using equation (15), and the dashed curve from a direct NRG calcu-

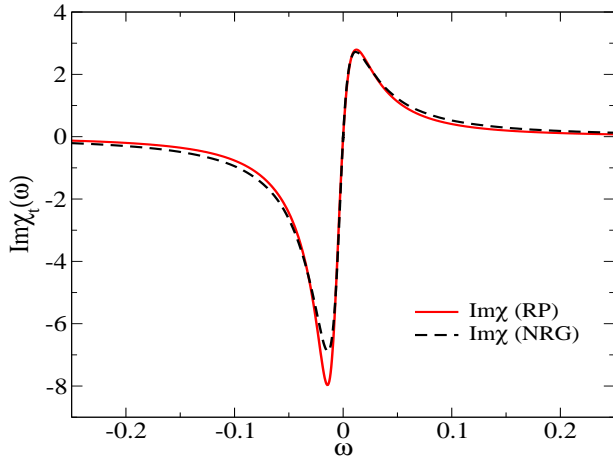


FIG. 6: The imaginary part of the transverse dynamic susceptibility, $\chi_t(\omega, h)$ at $T = 0$ as a function of ω , for the asymmetric Anderson model for $h/\pi\Delta = 0.04$ and the same set of parameters as given in figure 1.

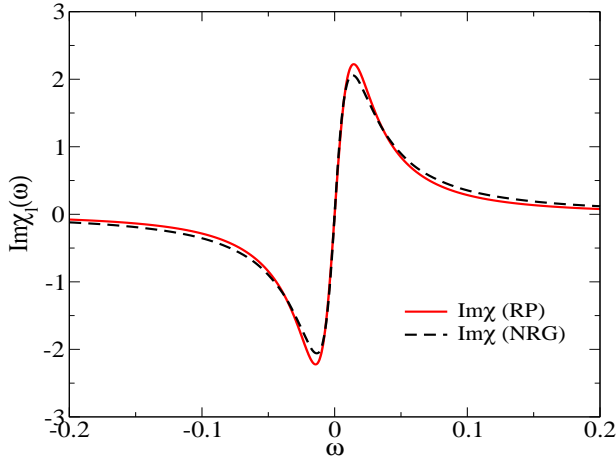


FIG. 7: The imaginary part of the longitudinal dynamic susceptibility, $\chi_l(\omega, h)$ at $T = 0$ as a function of ω , for the asymmetric Anderson model for the same parameters and magnetic field value ($h/\pi\Delta = 0.04$) as given in figure 6.

lation. The peak positions are in good agreement, and the slightly broader peak from the NRG data can be attributed to the logarithmic broadening used in the direct NRG evaluation. There is a sum rule, that the total spectral weight is equal to $-2m(h)$, which is satisfied precisely both in the RPT result and also in the NRG calculation, as we have used the improved prescription for the response functions based on the complete Anders-Schiller basis. The imaginary part of the corresponding dynamic longitudinal susceptibility $\chi_l(\omega, h)$ for this value of the magnetic field is shown in figure 7. Due to the stronger magnetic field, the peaks are somewhat suppressed as compared with the results shown in figure for $h/\pi\Delta = 0.001$, but the overall features are very similar. The spectral densities, $\rho_\uparrow(\omega)$ and $\rho_\downarrow(\omega)$, for this field ($h/\pi\Delta = 0.04$) are shown in figure 8. As the polarization is much stronger for this higher magnetic field

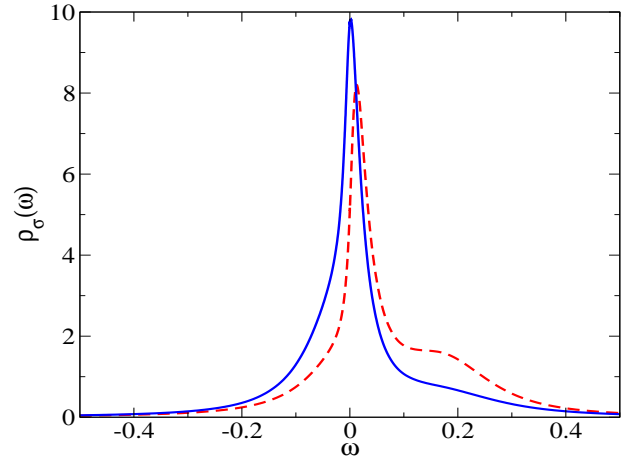


FIG. 8: The spectral density for the spin up electrons $\rho_\uparrow(\omega, h)$ (full curve) and spin down $\rho_\downarrow(\omega, h)$ (dashed curve) at $T = 0$ as a function of ω for the same set parameters and magnetic field value as used for the plot of $\chi_t(\omega, h)$ in figure 7.

value, there is now a marked difference between the two spectral densities for the two spin types.

In summary, the results of this section for the impurity models away from particle-hole symmetry display new features, such as the spin dependent resonance widths in the quasiparticle density of states. We show that the magnetisation and the static response functions can be well described in terms of the field dependent renormalized parameters. We have used these parameters to calculate the dynamic longitudinal and transverse spin susceptibilities in the RPT formulae and we find excellent results when compared with those obtained from a direct NRG calculation.

III. INFINITE DIMENSIONAL HUBBARD MODEL

In this section we turn our attention to lattice models with a local interaction terms and in particular to the infinite dimensional Hubbard model. The Hubbard model has played a similar role for lattice models as the Anderson model for impurity models, being the simplest model of its type, where the interplay of kinetic energy and strong local interactions can be studied.

A. Dynamical mean field approach and renormalized parameters

The Hamiltonian for the model in a magnetic field is given by

$$H = - \sum_{i,j,\sigma} (t_{ij} c_{i,\sigma}^\dagger c_{j,\sigma} + \text{h.c.}) - \sum_{i\sigma} \sigma h n_{i\sigma} + U \sum_i n_{i,\uparrow} n_{i,\downarrow}, \quad (17)$$

where t_{ij} are the hopping matrix elements between sites i and j , U is the on-site interaction.

From Dyson's equation, the Green's function $G_{\mathbf{k},\sigma}(\omega)$ can be expressed in the form,

$$G_{\mathbf{k},\sigma}(\omega) = \frac{1}{\omega + \mu_\sigma - \Sigma_\sigma(\mathbf{k}, \omega) - \varepsilon(\mathbf{k})}, \quad (18)$$

where $\Sigma_\sigma(\mathbf{k}, \omega)$ is the proper self-energy, and $\varepsilon(\mathbf{k}) = \sum_{\mathbf{k}} e^{-\mathbf{k} \cdot (\mathbf{R}_i - \mathbf{R}_j)} t_{ij}$, $\mu_\sigma = \mu + \sigma h$, with the chemical potential μ . The simplification that occurs for the model in the infinite dimensional limit is that $\Sigma_\sigma(\mathbf{k}, \omega)$ becomes a function of ω only^{26,27}. In this case the local Green's function $G_\sigma^{\text{loc}}(\omega)$ can be expressed in the form,

$$G_\sigma^{\text{loc}}(\omega) = \sum_{\mathbf{k}} G_{\mathbf{k},\sigma}(\omega) = \int d\varepsilon \frac{D(\varepsilon)}{\omega + \mu_\sigma - \Sigma_\sigma(\omega) - \varepsilon}, \quad (19)$$

where $D(\varepsilon)$ is the density of states for the non-interacting model ($U = 0$). It is possible to convert this lattice problem into an effective impurity one²⁸ and write this Green's function in the form,

$$G_\sigma^{\text{loc}}(\omega) = \frac{1}{\mathcal{G}_{0,\sigma}^{-1}(\omega) - \Sigma_\sigma(\omega)}, \quad (20)$$

where

$$\mathcal{G}_{0,\sigma}^{-1}(\omega) = G_\sigma^{\text{loc}}(\omega)^{-1} + \Sigma_\sigma(\omega). \quad (21)$$

The Green's function $G_\sigma^{\text{loc}}(\omega)$ can be identified with the Green's function $G_\sigma(\omega)$ of an effective Anderson model, by re-expressing $\mathcal{G}_{0,\sigma}^{-1}(\omega)$ as

$$\mathcal{G}_{0,\sigma}^{-1}(\omega) = \omega + \mu + \sigma h - K_\sigma(\omega), \quad (22)$$

so that

$$G_\sigma(\omega) = \frac{1}{\omega - \varepsilon_{d\sigma} - K_\sigma(\omega) - \Sigma_\sigma(\omega)}, \quad (23)$$

with $\varepsilon_{d\sigma} = -\mu_\sigma$. The function $K_\sigma(\omega)$ plays the role of a dynamical mean field describing the effective medium surrounding the impurity. In the impurity case in the wide band limit we have $K_\sigma(\omega) = -i\Delta$. Here as can be seen from equations (21) and (20), $K_\sigma(\omega)$ is a function of the self-energy $\Sigma_\sigma(\omega)$, and hence depends on σ . As this self-energy is identified with the impurity self-energy, which will depend on the form taken for $K_\sigma(\omega)$, it is clear that this quantity has to be calculated self-consistently. Starting from an initial form for $K_\sigma(\omega)$, $\Sigma_\sigma(\omega)$ is calculated using an appropriate 'impurity solver' from which $G_\sigma^{\text{loc}}(\omega)$ can be calculated using equation (19), and a new result for $K_\sigma(\omega)$ from equations (21) and (22). This $K_\sigma(\omega)$ serves as an input for the effective impurity problem and the process is repeated until it converges to give a self-consistent solution. These equations constitute the dynamic mean field theory (DMFT), and further details can be found in the review article of Georges et al.²⁸.

Of the many impurity solvers the most commonly used are the Monte Carlo, the Exact diagonalization (ED) method and the NRG, all of which have advantages and disadvantages. Here, we wish to calculate the field dependent renormalized parameters to describe the quasi-particles, as we did for the Anderson model, so we use the NRG approach. It is also the most accurate method for calculations at $T = 0$ and for the low energy excitations. There has been a DMFT study of the static properties of a half-filled Hubbard model in a magnetic field using the ED method by Laloux et al.⁶. The focus of our paper here, however, is rather different so there is little overlap with this earlier work but, where there is, we make comment and compare with their results.

We need to specify the density of states $D(\omega)$ of the non-interacting infinite dimensional model, which is usually taken to be either for a tight-binding hypercubic or Bethe lattice. Here we take the semi-elliptical form corresponding to a Bethe lattice,

$$D(\omega) = \frac{2}{\pi D^2} \sqrt{D^2 - (\omega + \mu_0)^2} \quad (24)$$

where $2D$ is the band width, with $D = 2t$ for the Hubbard model, and μ_0 the chemical potential of the free electrons. We choose this form, rather than the Gaussian density of states of the hypercubic lattice, as it has a finite bandwidth.

In the NRG approach²⁰ the conduction band is logarithmically discretized and the model then converted into the form of a one dimensional tight binding chain, coupled via an effective hybridization V_σ to the impurity at one end. In this representation $K_\sigma(\omega) = |V_\sigma|^2 g_{0,\sigma}(\omega)$, where $g_{0,\sigma}(\omega)$ is the one-electron Green's function for the first site of the isolated conduction electron chain. If we use this form in equation (23), and expand the self-energy $\Sigma_\sigma(\omega)$ to first order in ω , we can write the result in the form,

$$G_\sigma(\omega) = \frac{z_\sigma}{\omega - \tilde{\varepsilon}_{d\sigma} - |\tilde{V}_\sigma|^2 g_{0,\sigma}(\omega) + O(\omega^2)}, \quad (25)$$

where

$$\tilde{\varepsilon}_{d\sigma} = z_\sigma(\varepsilon_{d\sigma} + \Sigma_\sigma(0)), \quad |\tilde{V}_\sigma|^2 = z_\sigma |V_\sigma|^2, \quad (26)$$

where $z_\sigma = 1/(1 - \Sigma'_\sigma(0))$, very similar to the result in equation (4). We can interpret this result as a free quasi-particle propagator, $\tilde{G}_{0,\sigma}(\omega)$, given by

$$\tilde{G}_{0,\sigma}(\omega) = \frac{1}{\omega - \tilde{\varepsilon}_{d\sigma} - |\tilde{V}_\sigma|^2 g_{0,\sigma}(\omega)}, \quad (27)$$

and z_σ as the quasiparticle weight. A similar Fermi liquid expansion in (19) leads to

$$\tilde{G}_{0,\sigma}^{\text{loc}}(\omega) = \int d\varepsilon \frac{D(\varepsilon/z_\sigma)}{\omega + \tilde{\mu}_{0,\sigma} - \varepsilon}, \quad (28)$$

where $\tilde{\mu}_{0,\sigma} = z_\sigma(\mu_\sigma - \Sigma_\sigma(0))$. In the DMFT approach we identify

$$\tilde{G}_{0,\sigma}^{\text{loc}}(\omega) = \tilde{G}_{0,\sigma}(\omega), \quad (29)$$

which specifies the form of $g_{0,\sigma}(\omega)$ in (27) and yields $\tilde{\mu}_{0,\sigma} = -\tilde{\varepsilon}_{d\sigma}$. We can define a density of states $\tilde{\rho}_{0,\sigma}(\omega)$ for the free quasiparticles via $\tilde{\rho}_{0,\sigma}(\omega) = -\text{Im}\tilde{G}_{0,\sigma}(\omega + i\delta)/\pi$. For the Bethe lattice, this takes the form of a band with renormalized parameters,

$$\tilde{\rho}_{0,\sigma}(\omega) = \frac{2}{\pi\tilde{D}_\sigma^2} \sqrt{\tilde{D}_\sigma^2 - (\omega + \tilde{\mu}_{0,\sigma})^2}. \quad (30)$$

where $\tilde{D}_\sigma = z_\sigma D$.

We can deduce the renormalized parameters $\tilde{\varepsilon}_{d\sigma}$ and \tilde{V}_σ from the low lying excitations calculation from the the NRG using a generalization of the method given in an earlier paper¹². The quasiparticle weight z_σ is then obtained from the relation $z_\sigma = |\tilde{V}_\sigma/V_\sigma|^2$ in equation (26).

We can define a quasiparticle occupation number \tilde{n}_σ^0 by integrating this density of states up to the Fermi level,

$$\tilde{n}_\sigma^0 = \int_{-\infty}^0 d\omega \tilde{\rho}_{0,\sigma}(\omega). \quad (31)$$

Using Luttinger's theorem²⁹ it is possible to relate this free quasiparticle occupation number \tilde{n}_σ^0 to the expectation value of the occupation number n_σ in the interacting system at $T = 0$. Using the quasiparticle density of states in equation (30), we can rewrite equation (31) as

$$\tilde{n}_\sigma^0 = \int_{-\infty}^0 d\omega D(\omega) \theta(\mu_\sigma - \Sigma_\sigma(0) - \omega), \quad (32)$$

where $\theta(\omega)$ is the Heaviside step function and $D(\omega)$ as given in equation (24). Then from Luttinger's result the right-hand side of equation (32) is equal to n_σ . We then have the result,

$$\tilde{n}_\sigma^0 = n_\sigma, \quad (33)$$

that the occupation for electrons of spin σ is equal to the number of free quasiparticle of spin σ , as calculated from equation (31). It should be noted that there is no simple generalization of the $h = 0$ result, $\mu - \mu_0 = \Sigma(0)$, in the spin polarized case.

We can also calculate the local longitudinal and transverse dynamic spin susceptibilities, $\chi_l(\omega)$ and $\chi_t(\omega)$, for this model using equations, (13) and (15), derived earlier in the impurity case. The free quasiparticle susceptibilities $\tilde{\chi}_{\sigma,\sigma'}(\omega)$ required are calculated using the local free quasiparticle density of states $\tilde{\rho}_{0,\sigma}(\omega)$ given in equation (30). We can calculate the local on-site quasiparticle interaction \tilde{U} as in the impurity case, but we do not have the simple formula relating \tilde{U} to $\chi_l(0)$ and $\chi_t(0)$ that enabled us to deduce the irreducible quasiparticle interactions \tilde{U}_l and \tilde{U}_t ; the impurity formula we used earlier is only valid in the wide band limit. To determine \tilde{U}_l and \tilde{U}_t in the lattice case we use the condition that $\text{Re}\chi_l(\omega)$ and $\text{Re}\chi_t(\omega)$ fit the NRG result at the single point $\omega = 0$.

We can then compare the results based on these RPT formulae, which take into account the repeated quasiparticle scattering, with the NRG results over the whole frequency range.

Having covered the basic theory, we are now in a position to survey the results for the Hubbard model in different parameter regimes.

B. Results at Half-filling

We present the results at half-filling for three main parameters regimes where we find qualitatively different behavior. The results in all cases will be for a Bethe lattice with a band width $W = 2D = 4$, setting $t = 1$. In concentrating on the field induced polarization, we do not include the possibility of antiferromagnetic ordering. The regimes are a relatively weak coupling regime (a) where U is smaller than the band width, an intermediate coupling regime (b) with $W < U < U_c$, where U_c is the value at which a Mott-Hubbard gap develops in the absence of a magnetic field ($U_c \approx 5.88$), and (c) a strong coupling regime with $U > U_c$.

The first plot in figure 9 gives the spectral densities for the majority spin electrons $\rho_\uparrow(\omega)$ for various magnetic field values in the weakly correlated regime, $U = 2$. We

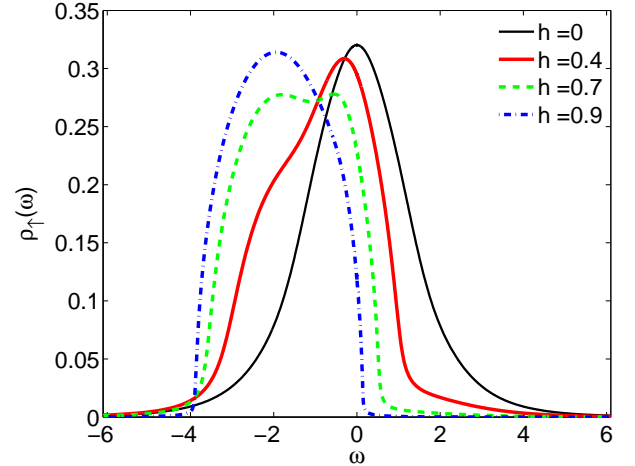


FIG. 9: The local spectral density for the majority spin $\rho_\uparrow(\omega)$ for $U = 2$ and various fields h .

can see clearly that, for increasing magnetic field, more and more spectral weight is shifted to lower energies (the opposite happens for the other spin component, which is not displayed here). Above $h \simeq 1.0$ the system is completely polarized, $2m = 1$. This extreme high field limit corresponds to an insulator; there is a gap of the magnitude $\Delta_g(h) = 2h + U - W$ between the upper (minority) and lower (majority) bands, which both have the semi-elliptical form as for non-interacting system with $W = 4$. The inverse of the quasiparticle weight $z_\sigma(h)$, which corresponds to the enhancement of the effective mass $m_\sigma^*(h) = m/z_\sigma(h)$, is shown as a function of h in fig. 10. The renormalized parameters (RP) $\tilde{\varepsilon}_{d,\sigma}$ and $|\tilde{V}_\sigma|^2$

were calculated from the NRG low energy excitations, as described in the previous section, and the values of $z_\sigma(h)$ deduced using equation (26). We also calculated $z_\sigma(h)$ from the numerical derivative of the NRG calculated self-energy $\Sigma_\sigma(\omega)$ for both spin up and spin down electrons. All values agree very well and $z_\uparrow(h) = z_\downarrow(h)$, as expected in the case with particle-hole symmetry. The method based on the renormalized parameters is only applicable in the metallic regime. The values of $z_\sigma(h)$ increase from about 0.75 to 1, which corresponds to a progressive “de-renormalization” of the quasiparticles with increasing field, as observed earlier for the impurity model¹⁰. Since the interaction term in the Hubbard model acts only for opposite spins it is clear that there is no renormalization when the system is completely polarized with one band fully occupied and the other empty. The expectation value of the double occupancy $\langle n_\uparrow n_\downarrow \rangle$ decreases with increasing field, which further illustrates why the interaction term becomes less important for larger fields.

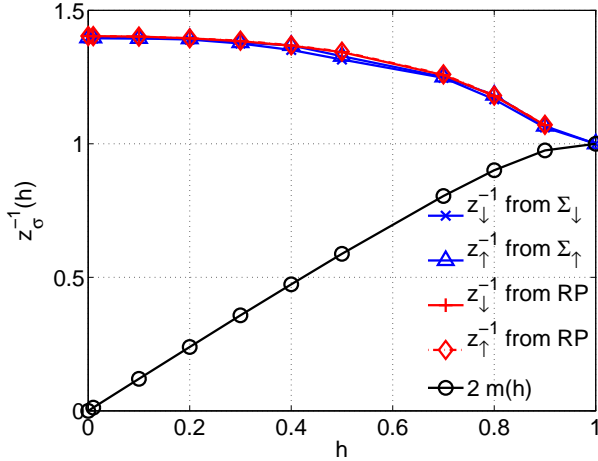


FIG. 10: The inverse of the quasiparticle weight $z_\sigma(h)$ calculated from renormalized parameters (RP) and directly from the self-energy and the magnetization $m(h)$ for $U = 2$ and various fields h .

We can also follow the field dependence of the renormalized chemical potential $\tilde{\mu}_{0,\sigma}(h)$ as shown in figure 11. It is shown deduced from the renormalized parameter (RP) $\tilde{\epsilon}_{d,\sigma}$ and as calculated directly from the self-energy. The agreement is very good over the full range of magnetic fields.

Mean field theory is valid for very weak interactions, so we compare our results for $\tilde{\mu}_{0,\sigma}(h)$ for $U = 2$, with the mean field value $\tilde{\mu}_{0,\sigma}^{\text{mf}} = \mu + \sigma h - U n_{-\sigma}^{\text{mf}}$ in figure 11. The results coincide for $h = 0$, when $\tilde{\mu}_{0,\sigma}^{\text{mf}} = 0$ and when the system becomes fully polarized at large field values, $\tilde{\mu}_{0,\sigma}^{\text{mf}} = -\sigma(U+h)$, but in general $\tilde{\mu}_{0,\sigma}^{\text{mf}} > \tilde{\mu}_{0,\sigma}(h)$. We also compare the mean field (MF) result for the field dependence of the magnetization $m(h)$ with the one obtained in the DMFT calculation in figure 12. The general behavior is similar, but the mean field theory without quantum fluctuations overestimates the magnetization, as one would expect.

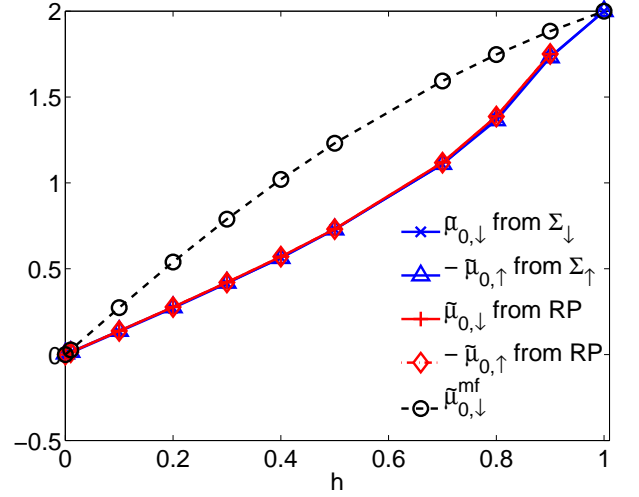


FIG. 11: The renormalized chemical potential $\tilde{\mu}_{0,\sigma}(h)$ calculated from renormalized parameters (RP) and directly from the self-energy for $U = 2$ and various fields h .

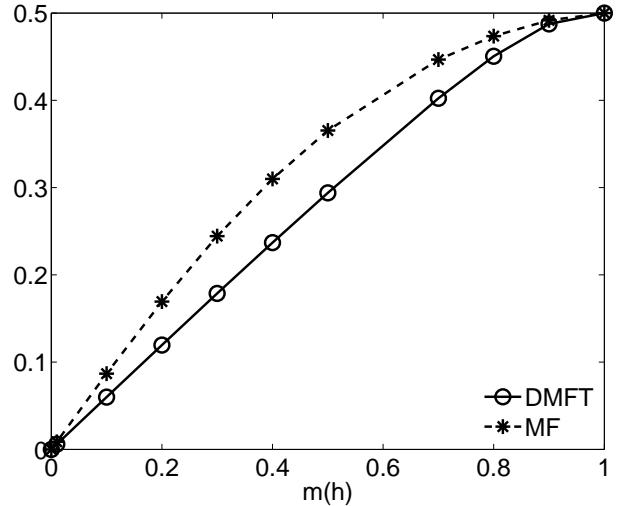


FIG. 12: The magnetization in the mean field approximation compared with the DMFT result for $U = 2$ and for the full range of magnetic fields h .

In the next plot in figure 13, where $U = 5$, we show typical behavior in the intermediate coupling regime. Similar to the weak coupling regime, we find a shift of spectral weight towards lower energy for the majority spin. There is, however, a difference in the way this happens due to the initial three peak structure, namely the quasiparticle peak in the middle gets narrower for increasing field and finally vanishes in the polarized phase. The quasiparticle weight, which is shown in figure 14, reflects this behavior by decreasing to zero with increasing field signaling heavy quasiparticles. When the material is polarized, however, the $z_\sigma(h)$ reverts to 1, which corresponds to the band insulator as before. This approach to the fully polarized localized state in high fields contrasts with that found in the weak coupling regime. It gives rise to metamagnetic behavior in this parameter regime.

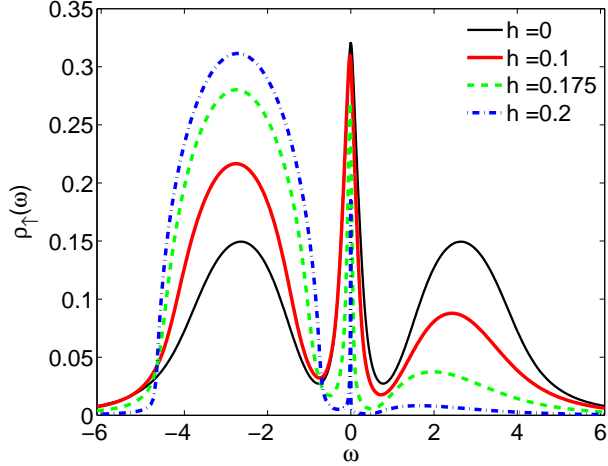


FIG. 13: The local spectral density for the majority spin $\rho_{\uparrow}(\omega)$ for $U = 5$ and various fields h .

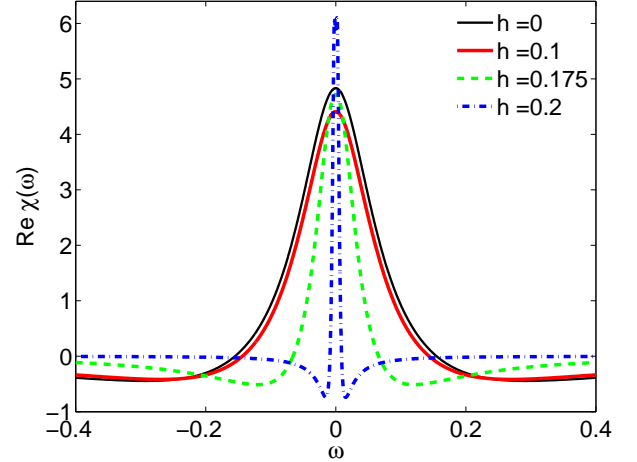


FIG. 15: The real part of the local longitudinal dynamic spin susceptibility for $U = 5$ and various fields h .

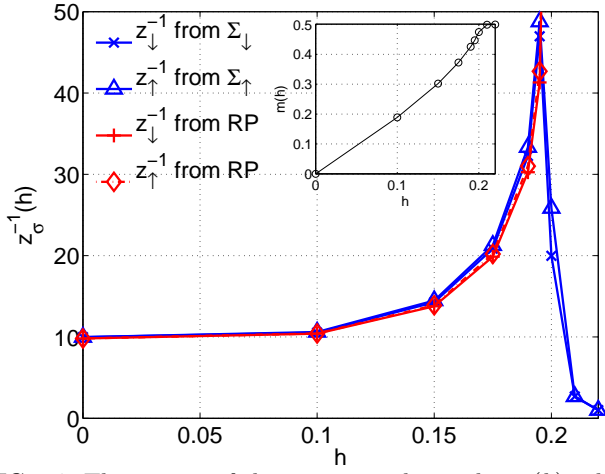


FIG. 14: The inverse of the quasiparticle weight $z_{\sigma}(h)$ calculated from renormalized parameters (RP) and directly from the self-energy for $U = 5$ and various fields h . The inset shows the magnetization $m(h)$.

To illustrate further this different response to a magnetic field, the real part of the local longitudinal dynamic spin susceptibility $\chi_l(\omega, h)$ as a function of ω is shown for various values of h . It can be seen that the local susceptibility $\chi^{\text{loc}}(h) = \text{Re } \chi_l(0, h)$ in this regime increases with h so that $\partial \chi^{\text{loc}}(h)/\partial h > 0$. This can also be seen in the curvature of the magnetization shown in the inset of figure 14. This is behavior characteristic of a metamagnetic transition and related to the magnetic field induced metal-insulator transition.

We can also check the Luttinger theorem in a magnetic field, as discussed in the previous section, by comparing the values of \tilde{n}_{σ}^0 , deduced from integrating the quasiparticle density of states with the value of n_{σ} calculated from the direct NRG evaluation in the ground state. These results are shown in figure 16. It can be seen that there is excellent agreement between the results of these two different calculations, $\tilde{n}_{\sigma}^0 = n_{\sigma}$, so that Luttinger's theorem is satisfied for all values of the magnetic field in this

intermediate coupling regime.

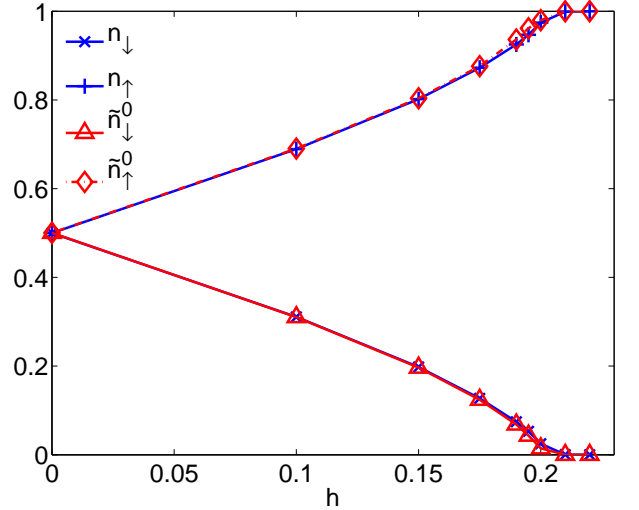


FIG. 16: The comparison of the spin dependent occupation numbers \tilde{n}_{σ}^0 and n_{σ} corresponding to Luttinger's theorem in a magnetic field for $U = 5$ and the range of fields h .

Finally we consider the strong coupling regime with $U > U_c$, where for $h = 0$ the spectral density has a Mott-Hubbard gap so that for half-filling the system is an insulator. The electrons will be localized with free magnetic moments coupled by an effective antiferromagnetic exchange $J \sim t^2/U$. In fields such that $h > J$, the system polarizes completely as can be seen in figure 17 where we show the total density of states $\rho(\omega) = \rho_{\uparrow}(\omega) + \rho_{\downarrow}(\omega)$ for $h = 0$ and $h = 0.2$. For smaller fields, such that $h < J$, we do not find a convergent solution to the DMFT equations, and the iterations oscillate between local states which are either completely full or empty. We interpret this as due to the tendency to antiferromagnetic order which in a weak field, due to the absence of anisotropy, will be almost perpendicular to the applied field in the x - y plane with a slight canting of the spins in the z -direction

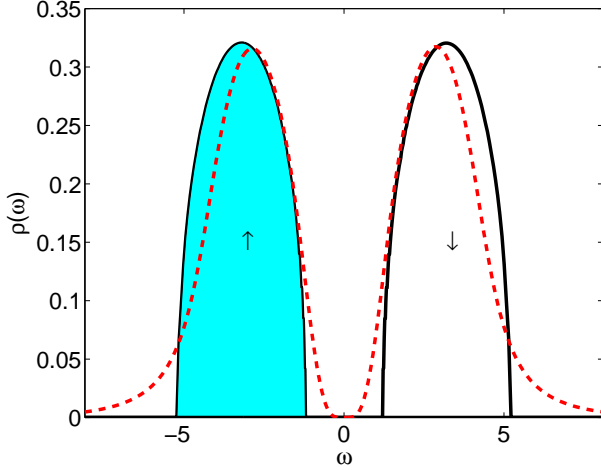


FIG. 17: The total local spectral density $\rho(\omega)$ for $U = 6$ for $h = 0$ (dashed line), Mott insulator, and $h = 0.2$ (full line), fully polarised band insulator.

(spin flopped phase). In this calculation no allowance has been made for this type of ordering, but this state can be well described using an effective Heisenberg model for the localized moments.

C. Quarter Filled Case

We now compare the results in the intermediate coupling regime with $U = 5$ at half-filling with those at quarter filling, $x = 0.5$, where the Fermi level falls in the lower Hubbard peak in the spectral density. To see how the band changes with increasing magnetic field we plot the density of states for both spin types, for the majority spin electrons in figure 18 and for the minority spin electrons in figure 19, for various values of the magnetic field.

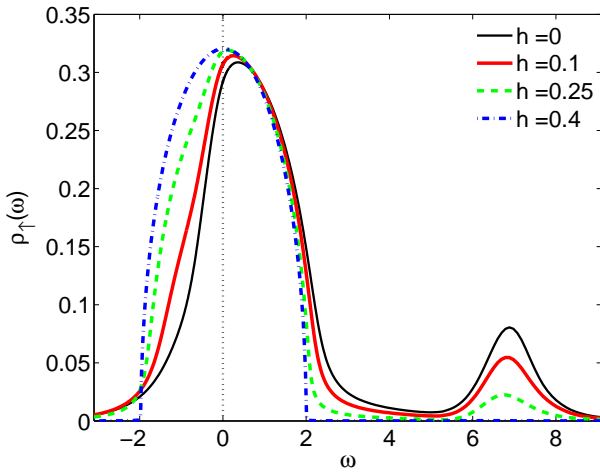


FIG. 18: The local spectral density for the majority spin $\rho_{\uparrow}(\omega)$ for $U = 5$, $x = 0.5$ and various fields h .

In the majority spin case the lower peak broadens on the low energy side and the weight in the upper peaks

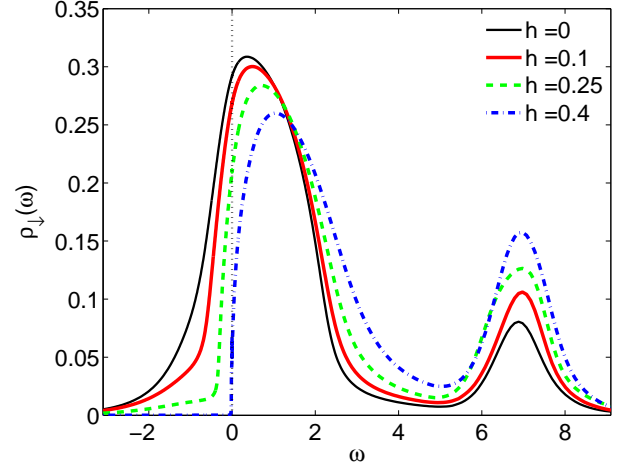


FIG. 19: The local spectral density for the minority spin $\rho_{\downarrow}(\omega)$ for $U = 5$, $x = 0.5$ and various fields h .

decreases with increase of the field. The opposite features can be seen in the minority spin case, with the spectral weight in the lower peak below the Fermi level decreasing and the weight in the upper peak increasing. Thus the increase of spectral weight below the Fermi level for the majority spin electrons, and the decrease for the minority spin electrons, can be seen to be due to a change of band shape rather than a simple relative shift of the two bands, which would be the case in mean field theory. In the fully polarized state there are no minority states below the Fermi level and the upper peak in the majority state density of states has disappeared.

The corresponding values for the inverse of the quasiparticle weight $1/z_{\sigma}(h)$ are shown in figure 20 for a range of fields. As noted in the impurity case, the quasiparticle weights differ for the two spin types with $z_{\uparrow}(h) > z_{\downarrow}(h)$. The values of $z_{\sigma}(h)$ have been calculated, as described earlier, both from the energy levels (RP) and from a numerical derivative NRG derived self-energy. There is reasonable agreement between the two sets of results, and the small differences to be seen be attributed to the uncertainty in the numerical derivative of the NRG self-energy. As in the impurity case, there is an initial decrease of $z_{\downarrow}(h)$ with increase of h , whereas $z_{\uparrow}(h)$ increases monotonically. The field dependence of the magnetization is also shown in figure 20, and is similar to the half-filled case with a weak interaction ($U = 2$). We have calculated, but do not show, the corresponding occupation values for \tilde{n}_{σ}^0 which again agree well with the values of \tilde{n}_{σ} , verifying Luttinger's theorem.

Our conclusion from these results, and from calculations with other values of U , is that when there is significant doping, the behavior in the field corresponds to a weakly correlated Fermi liquid, very similar to that at half-filling in the weak interaction regime. The only remarkable difference in the field is the spin dependence of the effective masses as shown in figure 20, which was already found similarly in the impurity case.

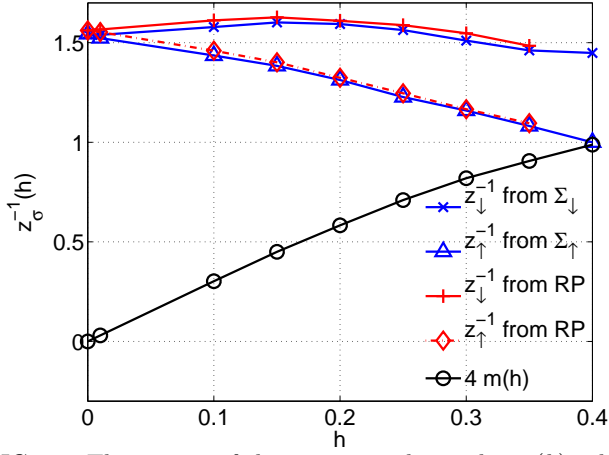


FIG. 20: The inverse of the quasiparticle weight $z_\sigma(h)$ calculated from renormalized parameters (RP) and directly from the self-energy for $U = 5$, $x = 0.5$ and various fields h . The magnetization $m(h)$ is also displayed.

D. Near half filling

Very close to half-filling and for large values of U we have a qualitatively different parameter regime. Here the system is metallic but we can expect strong correlation effects when U is of the order or greater than U_c , due to the much reduced phase space for quasiparticle scattering. We look at the case with 5% hole doping from half-filling and a value $U = 6$, which is just greater than the critical value for the metal-insulator transition. We show the spectral density of states for both the majority and minority spins states and various values of the magnetic field in figures 21 and 22, respectively. There is

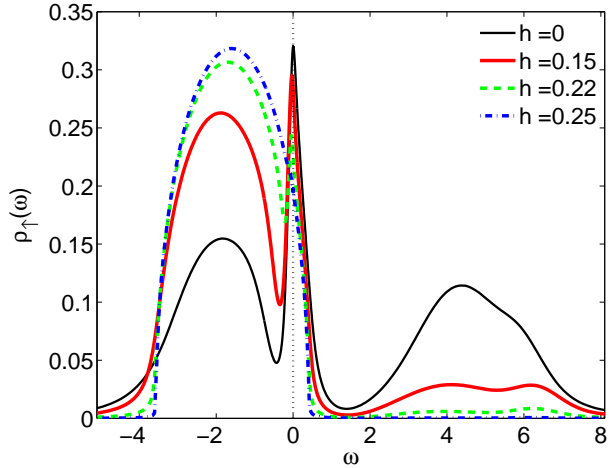


FIG. 21: The local spectral density for the majority spin $\rho_\uparrow(\omega)$ for $U = 6$, $x = 0.95$ and various fields h .

a clear sharp quasiparticle peak for $h = 0$ at the Fermi level at the top of the lower Hubbard band. As in the quarter filling case with $U = 5$ we see a similar transfer of spectral weight with increasing field to below the Fermi level for the majority spin case, and above the

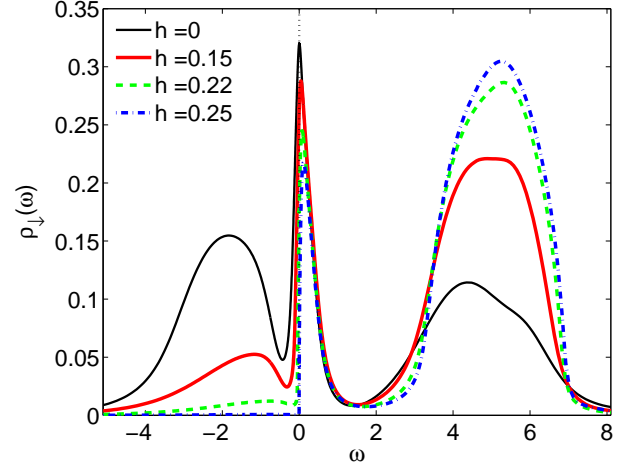


FIG. 22: The local spectral density for the minority spin $\rho_\downarrow(\omega)$ for $U = 6$, $x = 0.95$ and various fields h .

Fermi level for the minority spins. For large fields when the system is completely polarized there is still a sharp narrow peak in the spectral density of the minority spin states above the Fermi level, though the spectrum for the majority states below the Fermi level is that of the non-interacting system. A spin up electron added above the Fermi level feels no interaction as the system is completely spin up polarized so these electrons see the non-interacting density of states. On the other a spin down electron above the Fermi level interacts strongly with the sea of up spin electrons. The self-energy due to scattering with particle-hole pairs in the sea creates a distinct resonance in the down spin density of states just above the Fermi level. Just such a resonance was predicted by Hertz and Edwards³⁰ for a Hubbard model in a strong ferromagnetic (fully polarized) state.

The field dependence of the inverse of the quasiparticle weight is presented in figure 23. Again we find reason-

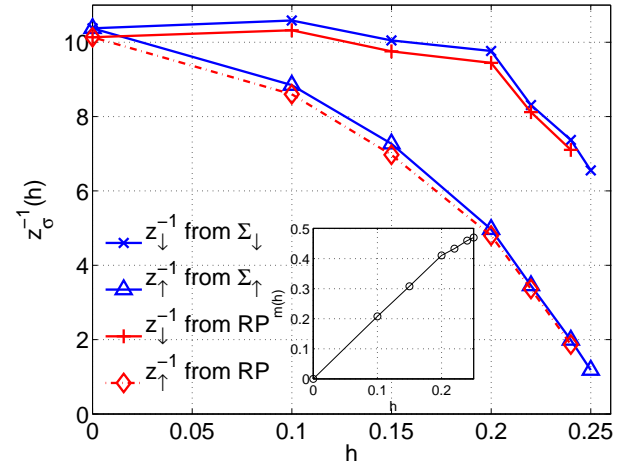


FIG. 23: The inverse of the quasiparticle weight $z_\sigma(h)$ calculated from renormalized parameters (RP) and directly from the self-energy for $U = 6$, $x = 0.95$ and various fields h . The inset shows the magnetization $m(h)$.

able agreement between the two methods of calculation for these quantities. The magnetization as a function of h is shown as an inset in the same figure. The behavior of $z_\uparrow(h)$ and $z_\downarrow(h)$ as a function of h contrasts sharply with the behavior found for the metallic state at half-filling with $U = 5$ shown in figure 14. For zero field the quasi-particle weight has a very similar value in both cases. At half-filling the tendency of the magnetic field to induce localization resulted in values of $z_\uparrow(h)$ and $z_\downarrow(h)$ ($z_\uparrow(h) = z_\downarrow(h)$) which decrease sharply as a function of h . In the 5% doped case with $U = 6$, the system must remain metallic and the quasiparticles weights, $z_\uparrow(h)$ and $z_\downarrow(h)$, both increase in large fields though their values differ significantly. The quasiparticle weight for the minority spin electrons decreases initially with increase of h , whereas that for the majority spins $z_\uparrow(h)$ increases monotonically and quite dramatically with h . When the system becomes fully polarized the up spin electrons become essentially non-interacting, $z_\uparrow(h) = 1$, whereas there is a strong interaction for a down spin electron and we find in this case $z_\downarrow(h) \simeq 0.15$. The interpretation for this is as given in the previous paragraph for the spectral densities.

We conclude that already a small doping of the system is enough to maintain a metallic character even for very strong interaction. Although the zero field spectra of the half filled case for $U = 5$ and the small doping case with $U = 6$ display very similar zero field behavior, i.e. a strongly renormalized quasiparticle band with similar z_σ , no field induced localization transition occurs for finite doping and no metamagnetic behavior is observed in the latter case.

IV. QUASIPARTICLE DYNAMICS

Having deduced the renormalized parameters of the quasiparticles from the NRG results presented in the previous section, we are now in a position to test how well we can describe the low energy dynamics of this model in a magnetic field in terms of a renormalized perturbation theory. We look at the various parameter regimes in turn.

A. Free quasiparticle spectral density

It is of interest first of all to see how the free quasiparticle density of states $\tilde{\rho}_\sigma(\omega)$ multiplied by $z_\sigma(h)$ compares with the spectral density $\rho_\sigma(\omega)$. In figure 24 we make a comparison in the zero magnetic field case. We see that the quasiparticle band gives a good representation of the low energy peak in $\rho_\sigma(\omega)$ and, as expected, does not reproduce the high energy features. These, however, to a fair approximation can be described by the mean field solution $\rho_{\text{mf}}(\omega)$ weighted with a factor $1 - z_\sigma$ as can be seen in figure 24. A case with a finite magnetic field $h = 0.15$, where the peaks in the density of states of the two spin species are shifted due to the induced polarization rela-

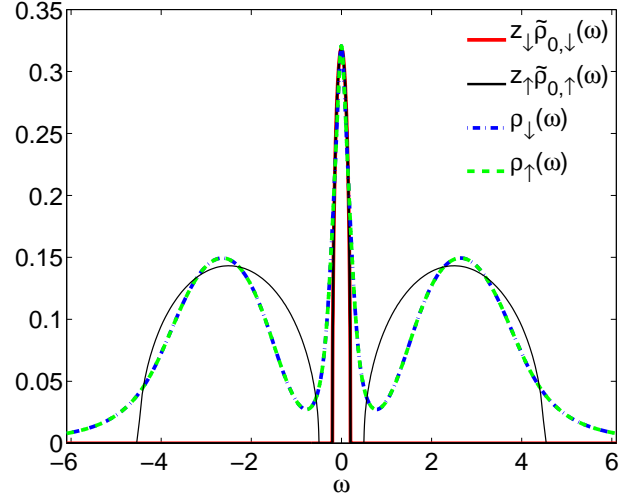


FIG. 24: The free quasiparticle density of states in comparison with interacting local spectral density for $U = 5$ and $h = 0$. We have also plotted a thin black line for $\rho_{\text{mf}}(\omega) = [D(\omega + U/2) + D(\omega - U/2)]/2$ which describes the non-magnetic mean field solution and weighted with $1 - z_\sigma$.

tive to the Fermi level, is shown in figure 25. The figure

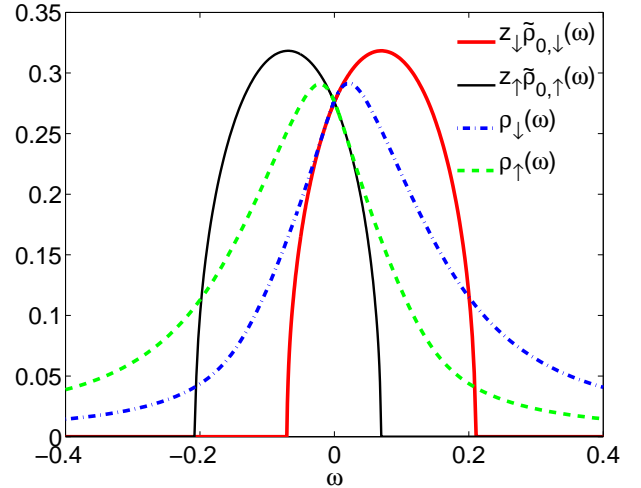


FIG. 25: The free quasiparticle density of states in comparison with interacting the local spectral density for $U = 5$ and $h = 0.15$.

focuses on the region at the Fermi level and one can see the the free quasiparticle density of states describes well the form of $\rho_\sigma(\omega)$ in the immediate vicinity of the Fermi level. It is to be expected that the frequency range for this agreement can be extended if self-energy corrections are included in the quasiparticle density of states using the renormalized perturbation theory as shown in the impurity case³¹.

In the fully polarized case with $h = 0.22$ there is complete agreement between the quasiparticle density of states and $\rho_\sigma(\omega)$ for both spin types as can be seen in the results shown in 26, where $z_\uparrow = z_\downarrow = 1$.

In figure 27 we show a fully polarized result ($h = 0.26$)

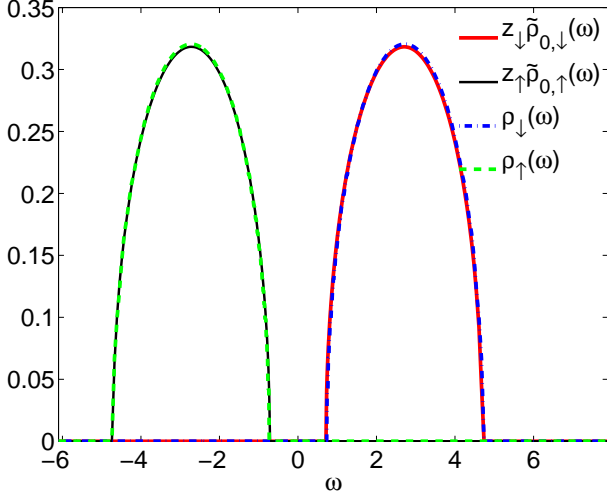


FIG. 26: The free quasiparticle density of states in comparison with interacting local spectral density for $U = 5$ and $h = 0.22$.

for the case near half filling, $x = 0.95$, $U = 6$ discussed in section III.D. We can see that the different values for

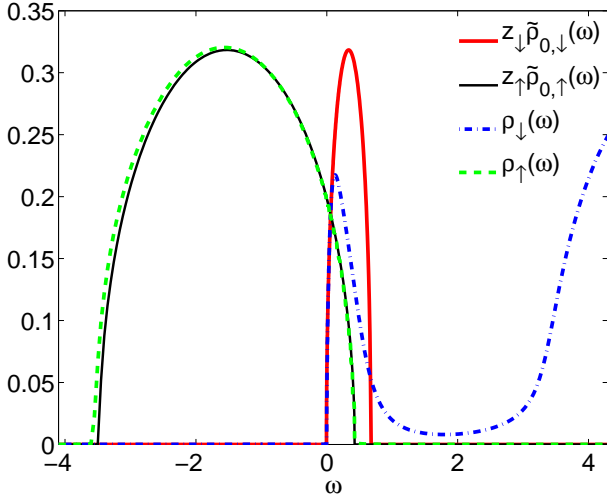


FIG. 27: The free quasiparticle density of states in comparison with interacting local spectral density for $U = 6$, $x = 0.95$ and $h = 0.26$.

the field dependent quasiparticle weight for up and down spin $z_\sigma(h)$ lead to remarkably different quasiparticle band shapes. With $z_\uparrow \simeq 1$ the majority spin quasiparticle band is essentially that of the non-interacting density of states. The very much smaller value z_\downarrow leads to a narrow quasiparticle band above the Fermi level. The low energy flank of this quasiparticle band describes well the narrow peak seen in the spectral density just above the Fermi level. To describe these strong asymmetries in the spectral densities near half filling, we need $z_\uparrow \gg z_\downarrow$, which contrasts with the cases at half filling such as in figures 25 and 26 where always $z_\uparrow = z_\downarrow$. This suggests a discontinuous behavior of the renormalisation factors z_σ on the approach to half filling.

B. Dynamic susceptibilities at Half-filling

We now compare the NRG results for the longitudinal and transverse local dynamic spin susceptibilities for the same value $U = 5$ and a similar range of magnetic field values with those based on the RPT formulae (13) and (15). In figure 28 we show the imaginary part of the transverse spin susceptibility calculated with the two different methods. It can be seen that RPT formula gives

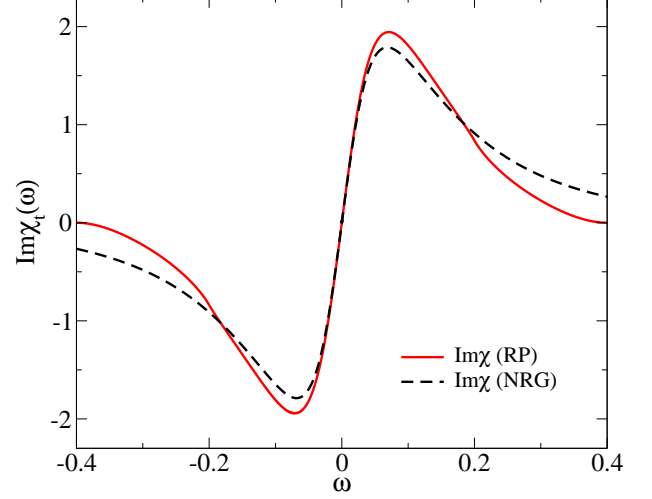


FIG. 28: A comparison of the imaginary parts of the transverse dynamic spin susceptibility for $U = 5$ and $h = 0.0$ calculated using the renormalized parameters (RP) and from a direct NRG calculation.

the overall form of the NRG results, and precisely fits the gradient of the NRG curve at $\omega = 0$. Some of the relatively small differences between the results might be attributed to the broadening factor used in the NRG results which gives a slower fall off with ω in the higher frequency range, and a slightly reduced peak. We get similar good agreement between the two sets of results for the same quantity for the case with a magnetic field $h = 0.15$, shown in figure 29.

In figure 30, where we give both the real and imaginary parts of the transverse susceptibility for $h = 0.19$, we see that this overall agreement is maintained in the large field regime where we get metamagnetic behavior. The shapes of the low energy peaks for both quantities are well reproduced by the RPT formulae. Note that the peak in the real part is not at $\omega = 0$, so it is not fixed by the condition that determines \tilde{U}_t , but nevertheless is in good agreement with the NRG results. Due to their very small values it becomes difficult to calculate $z_\sigma(h)$ as the system approaches localization for larger fields. In this regime as $z_\sigma(h) \rightarrow 0$ the free quasiparticle density of states will converge to a delta-function. Self-energy corrections to the free quasiparticle propagators, which were used in the calculation of $\tilde{\chi}_{\sigma,\sigma'}(\omega)$, will become increasingly important as this limit is approached. Once the system has localized, and is completely polarized, how-

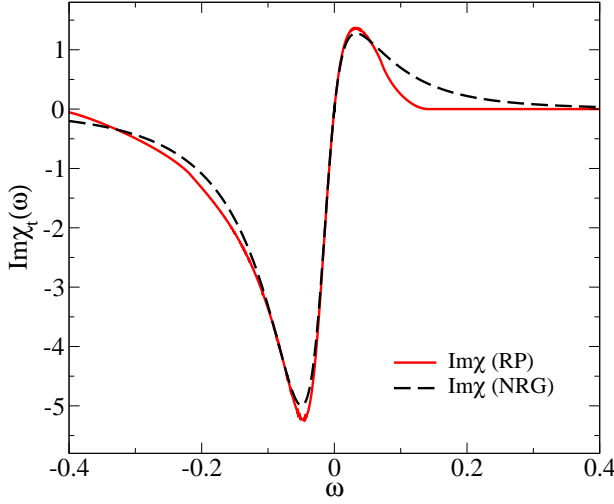


FIG. 29: Plots of the imaginary part of the transverse dynamic spin susceptibility for $U = 5$ and $h = 0.15$.

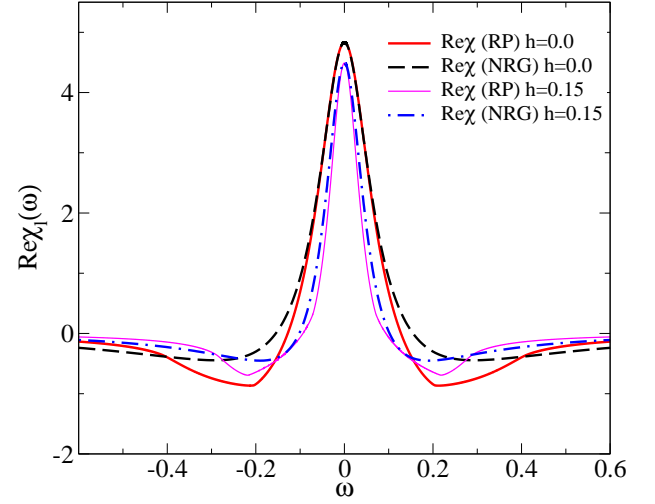


FIG. 31: The real part of the longitudinal dynamic spin susceptibility for $U = 5$ and $h = 0$ and $h = 0.15$.

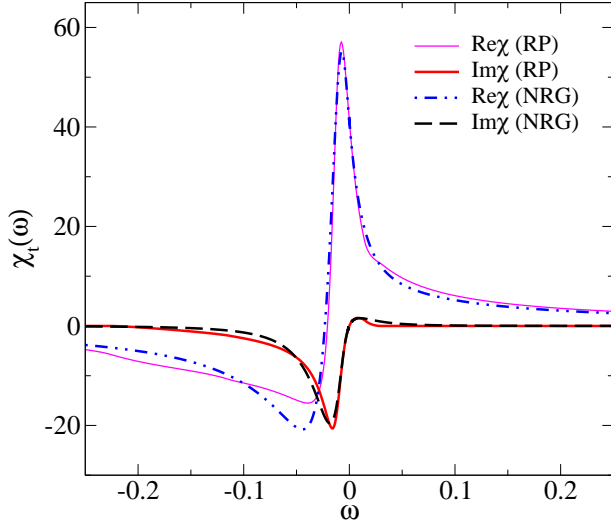


FIG. 30: The real and imaginary parts of the transverse dynamic spin susceptibility for $U = 5$ and $h = 0.19$.

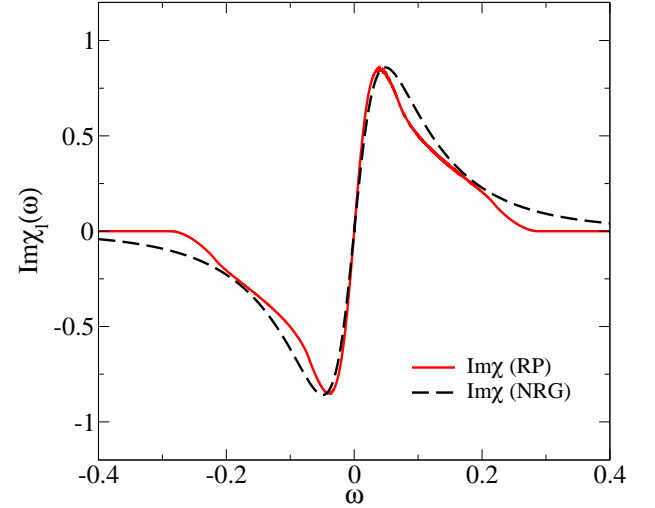


FIG. 32: The imaginary part of the longitudinal dynamic spin susceptibility for $U = 5$ and $h = 0.15$.

ever, we saw in figure 26 that the values deduced of $\tilde{\mu}_\sigma$ ($z_\sigma(h) = 1$) gave the a quasiparticle density of states coinciding with the NRG result.

Results for the longitudinal susceptibility are shown in figures 31 and 32. In figure 31 we give the values for the real part as a function of ω for $h = 0$ and $h = 0.15$. Here the peak height, which is at $\omega = 0$, is fixed by the condition which determines \tilde{U}_l . The width of the peaks in the two sets of NRG results, however, is given reasonably well by the RPT equations. The imaginary part of the longitudinal susceptibility obtained by the two methods is given in figure 32 for $h = 0.15$. Again there is overall agreement between the two sets of results. The slight undulations seen in the RPT results are due to the sharp cut off in the band edges in the free quasiparticle density of states. For larger values of h the agreement with the

NRG results is not as good as that as for the transverse susceptibility, and the central peak in the real part of the RPT results narrows more rapidly with h than in those obtained from the direct NRG calculation.

C. Dynamic susceptibilities at quarter filling

We give two examples of results for the susceptibilities for the model at quarter filling for the case $U = 5$ and $h = 0.1$. In figure 33 we give the real and imaginary parts for the transverse susceptibility. Despite the large value of U , we can see that the peak heights are very much reduced compared with those seen in the half-filled case for $U = 5$. The peak widths are also an order of magnitude larger as can be seen from the ω -scale. Nevertheless the RPT

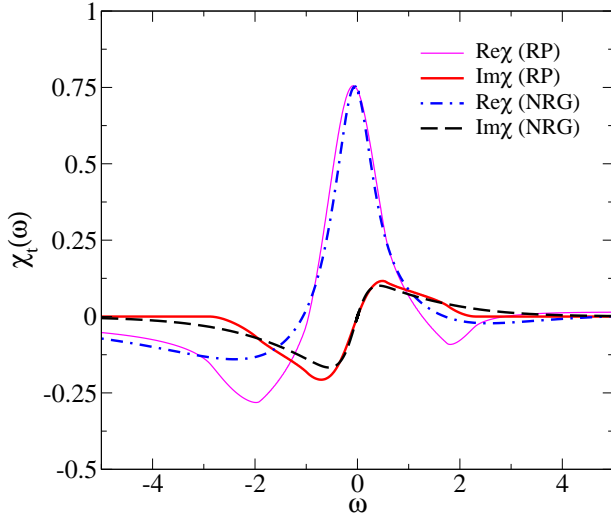


FIG. 33: The real and imaginary parts of the transverse dynamic spin susceptibility for $U = 5$, $x = 0.5$ and $h = 0.1$.

results reproduce well the overall features to be seen in the NRG results. The real and imaginary parts for the longitudinal susceptibility are shown in figure 33.

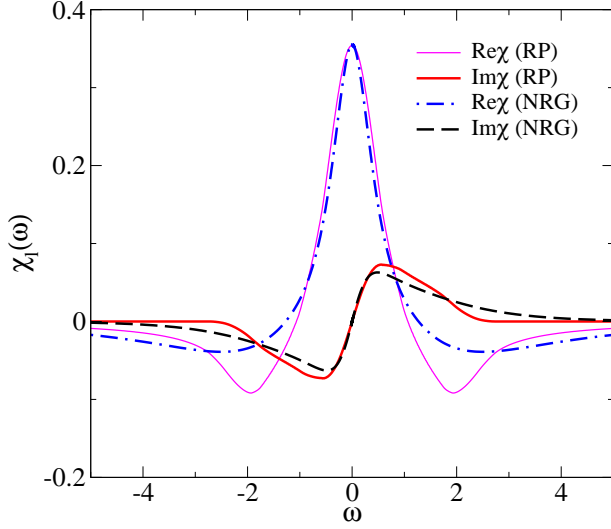


FIG. 34: The real and imaginary parts of the longitudinal dynamic spin susceptibility for $U = 5$, $x = 0.5$ and $h = 0.1$.

Again all the low energy features are reproduced in the RPT results. In this regime, apart from the overall factor of 2, there is less difference between the transverse and longitudinal susceptibilities than at half-filling.

D. Dynamic susceptibilities near half filling

Near half-filling ($x = 0.95$) we show plots for the two susceptibilities for parameters $U = 6$ and $h = 0.15$. In figure 35 we give the real and imaginary parts of the

transverse susceptibility. The low energy features are

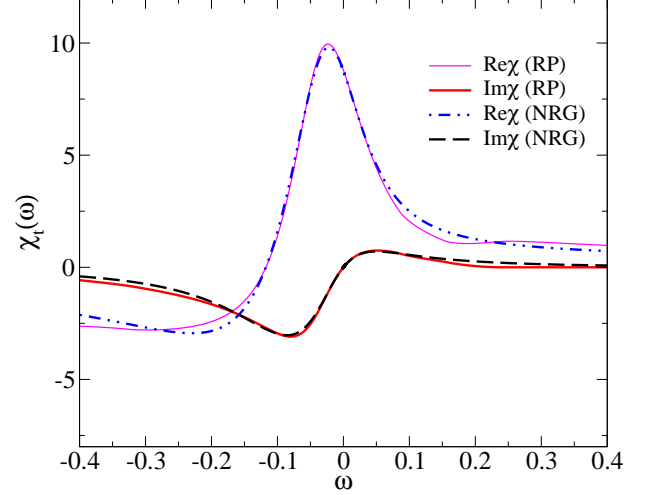


FIG. 35: The real and imaginary parts of the transverse dynamic spin susceptibility for $U = 6$, $x = 0.95$ and $h = 0.15$.

seen on an ω -scale an order of magnitude smaller than that for quarter filling due to the much stronger renormalization effects in this regime. There is excellent agreement both with the peak positions and shapes between the NRG and RPT results for both quantities. This is also seen to be the case for the real and imaginary part of the longitudinal susceptibility shown in figure 36, though the peak in the real part can be seen to be marginally narrower in the RPT results.

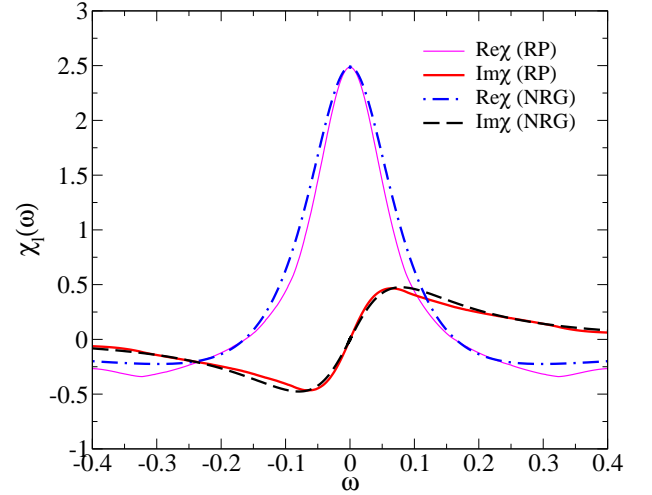


FIG. 36: The real and imaginary parts of the longitudinal dynamic spin susceptibility for $U = 6$, $x = 0.95$ and $h = 0.15$.

V. SUMMARY

In this paper we have extended our earlier work¹⁰, where we described the low energy behavior of the sym-

metric Anderson model in a magnetic field h in terms of field-dependent renormalized quasiparticles, to the non-symmetric Anderson model. The main new feature that emerges is the dependence of the quasiparticle peak resonance width $\tilde{\Delta}_\sigma(h)$ on the spin type σ as well as on the value of the magnetic field. The $T = 0$ spin and charge susceptibilities can be expressed as explicit formulae in terms of the parameters $\Delta_\sigma(h)$, $\tilde{\varepsilon}_{d,\sigma}(h)$ and a local field dependent interaction between the quasiparticles $\tilde{U}(h)$. It was also shown earlier for the symmetric model¹⁷, that an excellent description of the low energy spin dynamics can be obtained by taking into account repeated quasiparticle scattering in a renormalized perturbation theory (RPT). We have shown that these results can also be generalized to the non-symmetric model for the transverse and longitudinal spin susceptibilities, which again agree remarkably well with those obtained from a direct NRG calculation.

The method for calculating the field dependent quasiparticle parameters has also been extended here to infinite dimensional lattice models where the self-energy, as in the impurity case, is a function of frequency only. We have applied these methods to the Hubbard model to describe the low energy excitations in terms of a spin dependent renormalized quasiparticle band.

For the Hubbard model at half filling, where $z_\uparrow(h) = z_\downarrow(h)$, we presented results for the three main parameters regimes where the model displays qualitatively different behavior. Our results are on the whole consistent with those obtained earlier by Laloux et al.⁶ obtained using the ED method. An exception is in the insulating regime for weak fields, where we could not find a convergent solution of the DMFT equations. We attributed this to the fact that in this regime the magnetic field is smaller than the exchange coupling between the localized spins so that ground state would be one in which the spins would have a canted antiferromagnetic ordering in the plane perpendicular to the field.

Well away from half filling we find a magnetic response similar to the weakly correlated case even for large values of U . The large phase space for quasiparticle scattering in this regime leads to modest renormalization effects. Here, as in the impurity case, we find spin dependent quasiparticle weights, $z_\uparrow(h) \neq z_\downarrow(h)$. This implies spin dependent as well as field dependent effective masses, which have been discussed earlier in work by Spalek et al.^{4,32} and Riseborough³³. The calculations by Spalek et al. were based on a Gutzwiller³² and a mean-field slave boson approach⁴. We can make a comparison of our results (section III.D) near half filling, $x = 0.95$, with theirs in the later work⁴. We find a qualitatively similar behavior with the majority spin effective mass decreasing with h , but quantitatively there are differences. The field dependence of the minority spin effective mass $1/z_\downarrow(h)$ shows a very slow increase initially in both sets of results, but the large field behavior is quite different. As seen in figure 23 we find a significant decrease in $1/z_\downarrow(h)$ for large fields whereas the corresponding quantity in figure 3 in

reference⁴ increases.

The strong magnetic field dependence of the effective masses found in the calculations by Riseborough is based on the assumption that the system is close to a ferromagnetic transition (paramagnon theory). However, DMFT calculations for the Hubbard model find that any ferromagnetism in the Hubbard model only occurs in a very small region of the parameter space near half-filling and for very large values of U .³⁴ Our results are well away from this regime and the large effective masses obtained here can be attributed to the tendency to localization rather than the tendency to ferromagnetism.

Using the field dependent renormalized parameters $z_\sigma(h)$ and $\tilde{\mu}_\sigma(h)$ in the RPT formulae for the dynamic local longitudinal and transverse spin susceptibilities we found agreement with the overall features to be seen in the NRG results for these quantities. In the case of the transverse spin susceptibility excellent agreement was found in all the metallic regimes and for all values of the magnetic field considered, except in the high field regime at half filling as the localization point is approached, where consistent values of the renormalized parameters are difficult to calculate. The comparison of the RPT results with those from NRG was also excellent for the longitudinal dynamic susceptibility in the weaker field regime $h \leq 0.15$ but less good for higher fields, $h > 0.15$.

In all metallic parameter regimes a spin dependent Luttinger theorem in the form $n_\sigma = \tilde{n}_\sigma^0$, the number of particles equals the number of quasiparticles, was found to be satisfied for all strengths of the magnetic field. In this form it even holds in the fully polarized insulating state.

Phenomena like field and spin dependent effective masses and metamagnetic behavior have been observed experimentally in several heavy fermion compounds^{1,3,5,35}. The Hubbard model, however, being a one band model is not an appropriate starting point to make a quantitative comparison with the heavy fermion class of materials. A periodic Anderson model with a two band structure and including the degeneracy of the f electrons would be a better model to describe these materials. Field dependent effects in this model have been studied by several techniques, modified perturbation theory³⁶, exact diagonalization³⁷, $1/N$ expansion³⁸ and variational approach³⁹. The approach used here could be generalized to the periodic Anderson model, but restricted to the non-degenerate case and $N = 2$ as it is computationally too demanding in the NRG to deal with higher degeneracy. The Hubbard model at half filling has been used as a lattice model to describe the strongly renormalized Fermi liquid ^3He ^{6,7}. However, the metamagnetic behavior predicted for relevant parameter regime is not seen experimentally⁴⁰. In section III.D we found for small doping large effective masses, but no metamagnetic behavior. This raises the possibility that the weakly doped Hubbard model could serve as a basis for interpreting the experimental results for liquid ^3He .

Acknowledgement

We wish to thank N. Dupuis, D.M. Edwards, W. Koller, D. Meyer and A. Oguri for helpful discussions and W. Koller and D. Meyer for their contributions to the development of the NRG programs. One of us (J.B.) thanks the Gottlieb Daimler and Karl Benz Foundation, the German Academic exchange service (DAAD) and the EP-SRC for financial support.

VI. APPENDIX

The free quasiparticle dynamic susceptibility $\tilde{\chi}_{\sigma,\sigma'}(\omega)$ for the impurity model in the wide band limit, $\tilde{\Delta}_\uparrow = \tilde{\Delta}_\downarrow$, were given earlier¹⁷. Here we give the more general results for $\tilde{\Delta}_\uparrow \neq \tilde{\Delta}_\downarrow$,

$$\tilde{\chi}_{\sigma,\sigma}(\omega) = \frac{-1}{\pi\omega} \frac{\tilde{\Delta}_\sigma}{\omega - 2i\tilde{\Delta}_\sigma} \sum_{\alpha=-1,1} \ln \left(1 - \frac{\omega}{\alpha\tilde{\varepsilon}_{d,\sigma} + i\tilde{\Delta}_\sigma} \right), \quad (34)$$

for $\omega > 0$, and for $\omega = 0$,

$$\tilde{\chi}_{\sigma,\sigma}(0) = \tilde{\rho}_\sigma(0). \quad (35)$$

The values for $\omega < 0$ follow from the fact that $\text{Re}\tilde{\chi}_{\sigma,\sigma}(\omega) = \text{Re}\tilde{\chi}_{\sigma,\sigma}(-\omega)$ and $\text{Im}\tilde{\chi}_{\sigma,\sigma}(\omega) = -\text{Im}\tilde{\chi}_{\sigma,\sigma}(-\omega)$. For $\sigma' \neq \sigma$,

$$\begin{aligned} \tilde{\chi}_{\uparrow,\downarrow}(\omega) = & \frac{i/2\pi}{(\omega + \tilde{\varepsilon}_{d,\downarrow} - \tilde{\varepsilon}_{d,\uparrow} + i\tilde{\Delta}_\uparrow - i\tilde{\Delta}_\downarrow)} \ln \left(\frac{\omega - \tilde{\varepsilon}_{d,\uparrow} - i\tilde{\Delta}_\uparrow}{-i\tilde{\Delta}_\downarrow - \tilde{\varepsilon}_{d,\downarrow}} \right) \\ & + \frac{i/2\pi}{(\omega + \tilde{\varepsilon}_{d,\downarrow} - \tilde{\varepsilon}_{d,\uparrow} - i\tilde{\Delta}_\uparrow + i\tilde{\Delta}_\downarrow)} \ln \left(\frac{\omega + \tilde{\varepsilon}_{d,\downarrow} - i\tilde{\Delta}_\downarrow}{-i\tilde{\Delta}_\uparrow + \tilde{\varepsilon}_{d,\uparrow}} \right) \\ & + \frac{-i/2\pi}{(\omega + \tilde{\varepsilon}_{d,\downarrow} - \tilde{\varepsilon}_{d,\uparrow} + i\tilde{\Delta}_\uparrow + i\tilde{\Delta}_\downarrow)} \times \\ & \times \left[\ln \left(1 + \frac{\omega}{i\tilde{\Delta}_\uparrow - \tilde{\varepsilon}_{d,\uparrow}} \right) + \ln \left(1 + \frac{\omega}{i\tilde{\Delta}_\downarrow + \tilde{\varepsilon}_{d,\downarrow}} \right) \right]. \end{aligned}$$

-
- ¹ R. G. Goodrich, N. Harrison, A. Teklu, D. Young, and Z. Fisk, Phys. Rev. Lett. **82**, 3669 (1999).
 - ² W. Joss, J. M. van Ruitenbeek, G. W. Crabtree, J. L. Tholence, A. P. J. van Deursen, and Z. Fisk, Phys. Rev. Lett. **59**, 1609 (1987).
 - ³ H. Aoki, S. Uji, A. K. Albessard, and Y. Onuki, Phys. Rev. Lett. **71**, 2110 (1993).
 - ⁴ P. Korbel, J. Spalek, W. Wójcik, and M. Acquarone, Phys. Rev. B **52**, R2213 (1995).
 - ⁵ M. Manekar, S. Chaudhary, M. K. Chattopadhyay, K. J. Singh, S. B. Roy, and P. Chaddah, J. Phys.: Cond. Mat. **12**, 9645 (2000).
 - ⁶ L. Laloux, A. Georges, and W. Krauth, Phys. Rev. B **50**, 3092 (1994).
 - ⁷ D. Vollhardt, Rev. Mod. Phys. **56**, 99 (1984).
 - ⁸ V. Janis and G. Czycholl, Phys. Rev. B **61**, 9875 (2000).
 - ⁹ F. Kagawa, T. Itou, K. Miyagawa, and K. Kanoda, Phys. Rev. Lett. **93**, 127001 (2004).
 - ¹⁰ A. C. Hewson, J. Bauer, and W. Koller, Phys. Rev. B **73**, 045117 (2006).
 - ¹¹ P. W. Anderson, Phys. Rev. **124**, 41 (1961).
 - ¹² A. C. Hewson, A. Oguri, and D. Meyer, Eur. Phys. J. B **40**, 177 (2004).
 - ¹³ A. C. Hewson, *The Kondo Problem to Heavy Fermions* (Cambridge University Press, Cambridge, 1993).
 - ¹⁴ A. C. Hewson, J. Phys. Soc. Japan **74**, 8 (2005).
 - ¹⁵ A. C. Hewson, Phys. Rev. Lett. **70**, 4007 (1993).
 - ¹⁶ A. C. Hewson, J. Phys.: Cond. Mat. **13**, 10011 (2001).
 - ¹⁷ A. C. Hewson, J. Phys.: Cond. Mat. **18**, 1815 (2006).
 - ¹⁸ H. Shiba, Prog. Theor. Phys. **54**, 967 (1975).
 - ¹⁹ K. Wilson, Rev. Mod. Phys. **47**, 773 (1975).
 - ²⁰ H. R. Krishna-murthy, J. W. Wilkins, and K. G. Wilson, Phys. Rev. B **21**, 1003 (1980).
 - ²¹ O. Sakai, Y. Shimizu, and T. Kasuya, J. Phys. Soc. Japan **58**, 3666 (1989).
 - ²² T. A. Costi, A. C. Hewson, and V. Zlatić, J. Phys.: Cond. Mat. **6**, 2519 (1994).
 - ²³ R. Peters, T. Pruschke, and F. B. Anders (2006), cond-mat/0607494.
 - ²⁴ A. Weichselbaum and J. von Delft (2006), cond-mat/0607497.
 - ²⁵ F. B. Anders and A. Schiller, Phys. Rev. Lett. **95**, 196801 (2005).
 - ²⁶ W. Metzner and D. Vollhardt, Phys. Rev. Lett. **62**, 324 (1989).
 - ²⁷ E. Müller-Hartmann, Z. Phys. B **74**, 507 (1989).
 - ²⁸ A. Georges, G. Kotliar, W. Krauth, and M. Rozenberg, Rev. Mod. Phys. **68**, 13 (1996).
 - ²⁹ J. M. Luttinger, Phys. Rev. **119**, 1153 (1960).
 - ³⁰ J. A. Hertz and D. M. Edwards, Phys. Rev. Lett. **28**, 1334 (1972).
 - ³¹ J. Bauer, A. C. Hewson, and A. Oguri, J. Magn. Magn. Mat. (2006).
 - ³² J. Spalek and P. Gopalan, Phys. Rev. Lett. **64**, 2823 (1990).
 - ³³ P. S. Riseborough, Phil. Mag. **86**, 2581 (2006).
 - ³⁴ R. Zitzler, T. Pruschke, and R. Bulla, J. Phys.: Cond. Mat. **27**, 473 (2002).
 - ³⁵ S. V. Dordevic, K. S. D. Beach, N. Takeda, Y. J. Wang, M. B. Maple, and D. N. Basov, Phys. Rev. Lett. **96**, 017403 (2006).
 - ³⁶ D. Meyer and W. Nolting, Phys. Rev. B **64**, 052402 (2001).
 - ³⁷ T. Saso and M. Itoh, Phys. Rev. B **53**, 6877 (1996).
 - ³⁸ Y. Ono, J. Phys. Soc. Japan **67**, 2197 (1998).
 - ³⁹ D. Edwards and A. C. M. Green, Z. Phys. B **103**, 243 (1997).
 - ⁴⁰ G. Buu, A. Forbes, A. van Steenberg, S. Wieggers, O. Reményi, L. Puech, and P. Wolf, J. Low Temp. Phys. **110**, 311 (1998).